Fall 12-10-2015

THREE-DIMENSIONAL WIND SPEED AND FLUX MEASUREMENTS OVER A RAIN-FED SOYBEAN FIELD USING ORTHOGONAL AND NON-ORTHOGONAL SONIC ANEMOMETER DESIGNS

Taylor Thomas
University of Nebraska-Lincoln, taylorthomas06@gmail.com

THREE-DIMENSIONAL WIND SPEED AND FLUX MEASUREMENTS OVER A RAIN-FED SOYBEAN FIELD USING ORTHOGONAL AND NON-ORTHOGONAL SONIC ANEMOMETER DESIGNS

by

Taylor M. Thomas

A THESIS

Presented to the Faculty of

The Graduate College at the University of Nebraska

In Partial Fulfillment of Requirements

For the Degree of Master of Science

Major: Natural Resource Sciences

Under the Supervision of Professor Andrew E. Suyker

Lincoln, Nebraska

December, 2015

THREE-DIMENSIONAL WIND SPEED AND FLUX MEASUREMENTS OVER A RAIN-FED SOYBEAN FIELD USING ORTHOGONAL AND NON-ORTHOGONAL SONIC ANEMOMETER DESIGNS

Taylor M. Thomas M.S.
University of Nebraska, 2015
Adviser: Dr. Andrew E. Suyker

The eddy covariance method for estimating fluxes of trace gases, energy and momentum in the constant flux layer above a plant canopy fundamentally relies on accurate measurements of the vertical wind speed. This wind speed is typically measured using a three-dimensional ultrasonic anemometer. Previous studies comparing anemometers with orthogonal transducer sets to those with non-orthogonal transducer sets suggest differences in measured 3D wind speed components, particularly for a vertical component. These differences, attributed to additional flow distortion caused by the non-orthogonal transducer arrangement and support structure, directly affect fluxes of trace gases, energy and momentum. A field experiment was conducted over a rain-fed soybean field at the AmeriFlux site (US-Ne3) near Mead, Nebraska to quantify these differences. Ultrasonic anemometers featuring orthogonal transducer sets (ATI Vx Probe) and non-orthogonal transducer sets (Gill R3) collected high frequency wind vector and sonic temperature data. The non-orthogonal Gill R3 models underestimated sensible heat flux by 11% and friction velocity by 5% relative to the ATI Vx orthogonal design under the same atmospheric conditions. For two versions of an angle of attack correction developed for this non-orthogonal anemometer, neither adequately corrected the Gill R3 sensible heat fluxes compared to those measured using the orthogonal ATI Vx probe.

Acknowledgments

Thank you to Tom Lowman of the University of Nebraska - School of Natural Resources, Xiaomao Lin of Kansas State University, and my committee members for their time and guidance during the project.

Thank you to Jiahong Li, Israel Begashaw, James Kathilankal, Liukang Xu, Michael Gaura, Alicia Minzel, Greg Biggs and Bill Biggs at LI-COR Biosciences for generous support throughout my graduate program.

This work would not have been possible without the love and support of my family including my wife, mother, father, and sister.

Table of Contents

Chapter 1. Introduction

1.1 Anemometer transducer orientation and flow distortion

Great efforts are made when using the eddy covariance technique to maximize the accuracy of flux measurements: the physical structure of the sensors and their arrangement are quantified; multiple corrections are applied for imperfect sensor response to the turbulent flow in the constant flux layer; sensors are carefully calibrated and checked for performance; sensors are constructed and mounted to minimize flow distortion. Over the last few years, the eddy covariance science community has become aware of an issue that was largely addressed in the original design of sonic anemometers but has now re-emerged as an important factor for new designs of these sensors. Early sonic anemometers used an arrangement that directly measured the vertical (w) and horizontal components (u and v) of velocity (orthogonal axes). A flow distortion correction (e.g., see Wyngaard *et al*., 1985) was developed to account for presence of the structure affecting the measurement. More recent designs use axes that measure wind speed at non-orthogonal angles (i.e., no direct measurement of u, v, and w) and employ vector mathematics to resolve the vertical velocity (an indirect measurement). The evidence suggests this non-orthogonal design creates flow distortion that is not being accounted for, and as a result, underestimates vertical velocity and all eddy covariance fluxes.

The difference in fluxes/turbulent statistics measured when using the non-orthogonal and orthogonal anemometer design is being studied with the consensus that

the non-orthogonal arrangement is indeed causing issues. Multiple studies for anemometers with non-orthogonal transducer orientation (e.g., Nakai et al. 2006; Nakai and Shimoyama 2012; Nakai et al., 2014; Frank et al. 2012; Kochendorfer et al. 2012; Horst et al., 2015) have quantified the reduction in the magnitude of vertical wind velocity and subsequent underestimation of fluxes. The ideal sonic anemometer responds to wind which is not horizontal by recording the vertical and horizontal components of the wind vector U as $Usin(\alpha)$ and $Ucos(\alpha)$, respectively, where α is the angle of attack – the angle between the wind vector and horizontal plane). Figure 1-1 shows a schematic representation of the angle of attack (Weiss and Allen, 1976). This cosine relationship

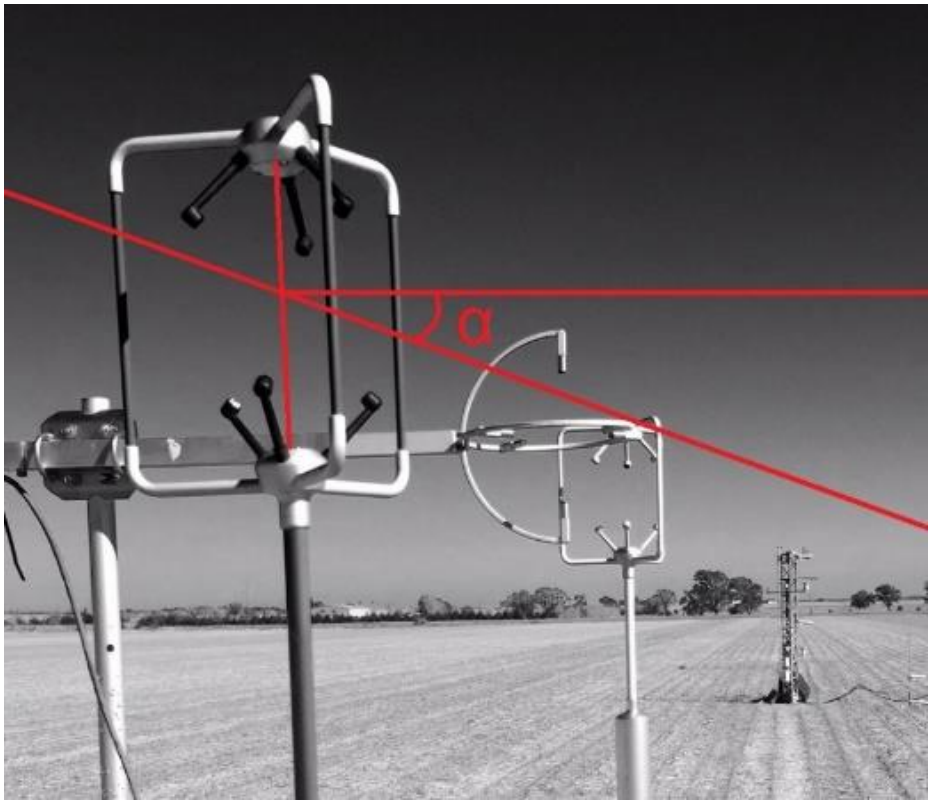

Figure 1-1. Schematic showing the definition of angle of attack for the sonic anemometer.

has been described in other studies including Christen et al. (2000) and Gash and Dolman (2003). Analyses such as in Nakai et al. (2006) demonstrate that a less than ideal (co)sine relationship likely due to flow distortion from the transducers and supporting structure of the anemometer. This impact is noted for both laminar (Nakai et al., 2006; Van der Molen et al., 2004) and turbulent flow conditions (Nakai et al., 2012; Frank et al., 2012; Kochendorfer et al., 2013; Nakai et al., 2014; Horst et al., 2015). The underestimation of fluxes/turbulent statistics of the surface layer flow have been consistent for multiple models of non-orthogonal sonic anemometers including the Gill Windmaster Pro/Gill R3 (Gill Instruments Ltd., Lymington, UK), CSAT3 (Campbell Scientific, Logan, Utah), and RM Young 81000VRE (R.M. Young, Traverse City, Michigan). Some studies compared data to those from an orthogonal anemometer and/or tilted non-orthogonal anemometer (thus altering the flow distortion). These studies show that the issue was clearly associated with the anemometer design. Some studies provided a correction to compensate for the underestimation of *w* (Nakai et al., 2006; Nakai and Shimoyama, 2012; Kochendorfer et al., 2012) so that users are able to more accurately reprocess high frequency eddy covariance data gathered with these types of anemometers. In other studies, the underestimation was simply shown to be present quantifying the effects on fluxes (e.g., Frank et al., 2012; Nakai et al., 2014). Table 1-1 presents a summary of the studies that have been performed recently to evaluate the angle of attack and induced flow distortion performance of commercially available non-orthogonal instruments. This underestimation of fluxes for these anemometers is likely related to the following three key issues.

Table 1-1. Summary of recent angle of attack/flow distortion impact studies. The non-orthogonal instrument is listed on the right, and the corresponding study is listed as employing either laminar or turbulent flow in its analyses.

Non-orthogonal Model	Wind Tunnel (Laminar)	Field (Turbulent)
Gill R2/R3	Nakai et al. 2006 Van der Molen et al. 2004	-
Gill Windmaster Pro	-	Nakai and Shimoyama 2012 Nakai et al., 2014
Campbell CSAT3	-	Frank et al. 2013 Horst et al., 2015
RM Young 81000	-	Kochendorfer et al. 2012

First, as the case with all sonic anemometers, there is flow distortion around a) the transducer and b) the support (mounting) structure for the transducer array. What complicates the dealing with this distortion for non-orthogonal sonic anemometers is the transformation of velocities in-line with the axes to "virtual" orthogonal axes. When this transformation is applied, orthogonal velocities include flow error/transducer shadowing in not one, but three axes (see Eqns.2-6 to 2-8, below). In addition, sonic temperature calculated from the speed of sound measurement (see Sec. 2.2.3) may be derived from multiple axes thus complicating its correction procedure (e.g., crosswind correction; Liu et al., 2001). Furthermore, the arrangement of the non-orthogonal transducers is unique among anemometer models. For example, the CSAT3 has the transducer pair oriented at 60^{o} from the horizontal. The Gill R3 sonic has the transducers orientated at 45^{o}. Therefore, the flow distortion may be different requiring a unique correction depending on the model in use.

The second issue is related to internal corrections applied by the respective firmware for each sonic anemometer. There are a number of calculations done

"internally" with the sonic firmware prior to measurements becoming recordable output. Many of these internal corrections are user selectable but some are not. For example, the Gill R3 units have a user-selectable "custom" calibration applied to horizontal wind velocity measurements to account for slight differences in anemometer structure. The calibration coefficients were derived from laminar flow in a wind tunnel. In addition, since 2006 and ending with firmware version v113, two Gill models (Windmaster and Windmaster Pro) were applying a digital-to-analog converter rolling average feature that acted as a low pass filter affecting frequencies as low as 1 (dimensionless frequency; see appendix A of Nakai et al., 2014 for more details). Furthermore, the 2006 and 2012 Nakai studies used omni-directional sonic anemometer models having the same physical structure. However, the estimated correction changed from 6% to 14% at a particular site (Nakai and Shimoyama, 2012). The larger correction term is probably linked to changes in the firmware between models. These kinds of issues further complicate quantifying the correction that should be applied to the non-orthogonal anemometers because these changes/errors in firmware get incorporated into equations attempting to correct the flow distortion. From a particular manufacturer, the angle of attack correction may depend on which model of anemometer is used and possibly which version of firmware was installed at the time of the measurements.

Thirdly, the measurement/biophysical/environmental conditions have to be considered when evaluating the impact on fluxes. This implies the absence of a simple correction factor associated with a particular anemometer. For example, Nakai et al. (2006) determined theoretical angle of attack corrections for Gill sonics in contrasting ecosystems with a range of canopy heights/zero plane displacements/roughness

parameters, and found sensible heat fluxes increased from about 6 to 15% (taller, rougher canopies tended to generate larger corrections). Other studies conducted under field conditions in contrasting ecosystems reported a similar range of systematic underestimation of "non-orthogonal sensible heat fluxes" (Nakai and Shimoyama, 2012: ~15%; Frank et al., 2012: ~8%; Kochendorfer et al., 2013: ~10% to 15%). However, for a particular ecosystem, a one to one comparison of the uncorrected and angle-of-attack-corrected flux had very high correlation coefficients ($r^2 > 0.99$; Nakai et al., 2014) with the intercept near zero suggesting a simple correction factor may be applied for a particular site as an alternative to reprocessing large amounts of eddy covariance data. The variation of the theoretical angle of attack correction in response to changes in measurement/biophysical/ environmental conditions would need to be evaluated at each site employing non-orthogonal anemometer design.

1.2 Impact of ultrasonic anemometer design on energy balance

The eddy covariance technique has historically had some issues with respect to closing the energy balance. The radiation from the sun drives the majority of natural processes at the Earth surface. A portion of the incident energy is reflected by the Earth surface, and remainder is available in the form of net radiation (*Rn*) for latent heat flux (*LE*), sensible heat flux (*H*), ground heat flux (*G*), the rate of change of heat storage in the air and biomass between the measurement location and the soil surface (*S*), and other energy sinks (Q) (Wilson et al., 2002). These energy exchange processes can be described for the Earth surface by the surface energy balance equation:

$$LE + H = Rn - G - S - Q \qquad \text{Eq. 1-1}$$

The surface energy balance equation shows that if the sensible and/or latent heat flux terms are not measured correctly, then the surface energy balance is not represented accurately resulting in a lack of closure between left and right sides of the equation 1-1 (Foken, 2008). Many eddy covariance sites around the globe report such a lack of closure (e.g., Baldocchi, 2003; Foken, 2008; Yuling, 2005) which is often used as a way to validate flux measurements at the sites. Systematic difference between the net radiation and the sum of other energy fluxes indicates a flaw in the experimental methodology for measurements of one or more of energy balance components (Wilson et al., 2002). The ultrasonic anemometer is an instrument that measures wind velocity and temperature, and represents an integral part of modern eddy-based techniques to quantify the two largest energy-consuming processes, sensible heat (*H*) and latent heat (*LE*) fluxes, as well as critical inputs required for calculations of other components, important variable and quality control parameters. The inclusion of an angle of attack correction increasing the magnitude of H and LE may have considerable impact on closing the energy balance across all ecosystems using non-orthogonal sonic anemometers.

1.3 Objectives

When using the eddy covariance method to estimate fluxes of energy and mass in the constant flux layer, correctly measuring the vertical component of three dimensional wind speed is of critical importance. The purpose of this study is to quantify the differences between an orthogonal and non-orthogonal ultrasonic anemometer with respect to the vertical wind speed and corresponding fluxes of sensible heat and momentum in the field experiment. Previous studies noted above have not employed this model of Gill with the most current version of internal corrections applied to the

measured data. In addition, we will examine the current "angle of attack" corrections available for the Gill R3 sonic anemometer by comparing corrected fluxes with those measured by an orthogonal sonic anemometer. To examine the effect of the physical structure of the orthogonal sonic anemometer beyond the transducers or support spars, an evaluation of the flow distortion caused by the support structure will also be presented. The overall goal of the experiment is to further understand the role of the ultrasonic anemometer design in the measurements of the vertical wind speed and fluxes calculated using the eddy covariance method.

Chapter 2. Review of Literature

2.1 Brief review of eddy covariance technique

The eddy covariance technique is a micrometeorological method to measure vertical turbulent fluxes *in situ* in the constant flux portion of the surface boundary layer by correlating the turbulent motion of air parcels with their corresponding characteristics such as air temperature, humidity, or gas concentration (Baldocchi et al., 2001; Baldocchi et al., 2003). The schematic representation (Fig. 2-1) indicates for the turbulent eddy on the left, the vertical windspeed *W1* moves the air parcel with (sonic) temperature *Ts1* downward. For the eddy on the right, the *W2* moves the air parcel with *Ts2* upward. Combined with air density and specific heat capacity of air at constant pressure, the difference in *Ts1* and *Ts2* generates a net movement of sensible heat energy.

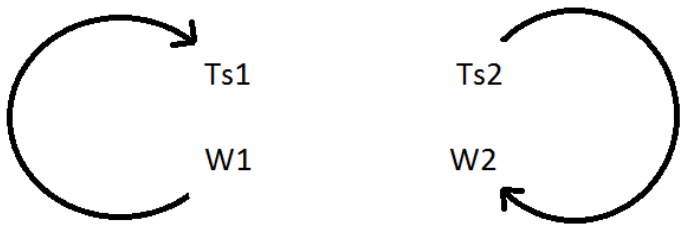

Figure 2-1. Conceptual representation of two turbulent eddies in the surface boundary layer with their respective wind speeds (*W1, W2*) and sonic anemometer air temperatures (*Ts1, Ts2*).

This method relies on the ability of the eddy covariance sensors to capture turbulent movement of eddies transporting the quantity of interest. Thus, rapid (i.e., 10 or 20 Hz), simultaneous, three dimensional measurements of wind speed with equally rapid measurements of the corresponding values of air temperature, humidity, and trace gas concentrations are required. Wind velocity and air temperature are typically measured

with a 3D ultrasonic anemometer while humidity and gas concentrations are measured with a "fast" time response gas analyzer (time constants greater than 0.1 s are preferred). As the sensors sample quickly, they capture the instantaneous turbulent flux (the product of a velocity and the quantity of interest). The eddy covariance technique requires a set of conditions including instrument location representative of the upwind footprint, negligible convergence or divergence of flow across the surface being measured, sufficiently turbulent conditions, and instrument height within the constant flux portion of the surface boundary layer, etc. (Burba, 2013). When these conditions are met, the flux reduces to a simple expression as the case for sensible heat flux (H):

$$H = \rho_a C_p \, \overline{w'T'} \qquad \text{Eq. 2-1}$$

where ρ_a is density of ambient air, C_p is the specific heat of air at constant pressure, w′ is the instantaneous deviation of vertical wind speed from an average value, and T′ is the instantaneous deviation of air temperature from an average value. The overbar denotes an average of the covariance product of the instantaneous w′T′. The average values are evaluated from data collected typically for a 30 or 60 minute duration. Over this period, enough eddies of different sizes have passed the measurement point to have adequately sampled the turbulence scales with significant contribution to the flux. Another important flux is that of momentum (u'w') often expressed via friction velocity (u_*), as follows:

$$. u* = (-\overline{u'w'})^{\frac{1}{2}} \qquad \text{Eq. 2-2}$$

where u′ is the fluctuation in horizontal velocity from its average value. All of these conditions were satisfied for the experiment or the data were not used (see Sec. 3.3).

2.2 Brief review of the development and function of the ultrasonic anemometer

2.2.1 Development

The concepts underlying the performance of an ultrasonic anemometer have been implemented into the construction of these sensors since the 1940's. The earliest predecessor of the modern sonic was constructed at Croft Laboratories at Harvard University. This instrument determined the velocity of the air parcel (wind speed) by determining the "phase difference between two microphones that were separated in space, upwind and downwind from a continuous source of sound" (Kaimal, 2013). This instrument featured four microphones located at the four cardinal directions. These sensors also measured phase shifts from a continuous source of sound. Compared with the mechanical, pressure and thermo-electric designs, this sonic model featured advantages, especially in applications where measuring the vertical component of wind speed was desirable, such as in the then-emerging techniques for measuring movement of energy and mass (Kaimal, 2013).

In 1960, J. Chandran Kaimal began developing a sonic anemometer/thermometer that featured two microphones mounted vertically to measure the phase shift between the signals. In 1964, Kaimal collaborated with the company "Bolt, Beranek and Newman" to develop a 3-axis sonic anemometer that could be deployed to simultaneously measure vertical and horizontal components of wind speed (Wyngaard et al., 1981; 1985). Further development resulted in the implementation of a "pulse system" as opposed to a "continuous wave system" as the latter had problems with "range and zero drift" (Izumi

at al., 1971). This finding represented an early instance of the possible effect of "transducer shadowing" on the measurement of wind speed (Kaimal, 2013; Wyngaard et al., 1985). As a result of these studies, a few companies developed commercially available ultrasonic anemometers. Today, multiple commercial ultrasonic anemometers are available and some have developed alternate designs for measuring turbulent wind speeds.

2.2.2 Function: velocity measurement

Ultrasonic anemometers employ ceramic, piezoelectric transducers (acting as both microphones and loud speakers) to emit and receive ultrasonic signals which travel through an air parcel moving through a fixed measurement path (D). The time it requires for the acoustic signal to travel from one transducer to another and be converted into an electronic signal on the receiving end is known as a transit time (T1). The acoustic signal is then sent in the opposite direction for a second transit time (T2). Each transducer is mounted inside a housing that, in turn, is supported by the frame of the anemometer in a fixed relative (orthogonal or non-orthogonal) geometry. The transit times for one pair of transducers are given as:

$$T1 = \frac{D}{C + V_d} \qquad \text{Eq. 2-3}$$

$$T2 = \frac{D}{C - V_d} \qquad \text{Eq. 2-4}$$

where C is the speed of sound in ambient air and V_d is the vector component of air flow resolved along the line of the pair of transducers. By inverting and subtracting, V_d is solved explicitly:

$$V_d = \frac{D}{2}\left[\frac{1}{T1} - \frac{1}{T2}\right] \quad \text{Eq. 2-5}$$

The expression for V_d is not affected by C or other parameters such as temperature or humidity (the impact of these parameters is implicitly incorporated in T1 and T2).

In many instrument designs, the transducer axes are not arranged on Cartesian coordinates, and thus aren't coincident with the usual Cartesian (or streamline or cardinal) axes that are typically associated with wind speeds. Furthermore, measured wind speed components in non-orthogonal geometries are not independent and must be transformed using the instrument's microprocessor into the U, V, and W component of wind velocity. For example, the following equations represent the transformation for the non-orthogonal Gill R3 100 and Gill R3 50 transducer configurations (refer to Gill R3 User's Manual):

$$U\ velocity = \frac{2a1 - a2 - a3}{2.1213} \quad \text{Eq. 2-6}$$

$$V\ velocity = \frac{a3 - a2}{1.2247} \quad \text{Eq. 2-7}$$

$$W\ velocity = \frac{a1 + a2 + a3}{2.1213} \quad \text{Eq. 2-8}$$

where a1, a2, and a3 are the axis velocities for these anemometers. Note the transformation is a function of the specific geometry of this model of sonic anemometer. Alternate designs require alternate equations.

2.2.3 Function: sonic temperature

The speed of sound in still air can be written as (Kaimal and Businger, 1963):

$$C = \left[\frac{\gamma R T_a}{M}\right]^{1/2} \quad \text{Eq. 2-9}$$

where γ is the ratio of the specific heats of air at constant volume and at constant pressure, R is the universal gas constant, M is the molecular weight of the ambient air, and T_a is the (actual) air temperature in Kelvin. From the transit times, the speed of sound can be computed by inverting and adding Eqs. 2-3 and 2-4 (Schotland, 1955):

$$C = \frac{D}{2}\left(\frac{1}{T1} + \frac{1}{T2}\right) \quad \text{Eq. 2-10}$$

Isolating T_a from Eq. 2-9 and substituting Eq, 2-10 gives:

$$T_s = \frac{D^2 M}{4\gamma R}\left(\frac{1}{T1} + \frac{1}{T2}\right)^2 \quad \text{Eq. 2-11}$$

where T_s is sonic temperature that differs from actual air temperature by an amount proportional to the water vapor content of the air measured. Schotanus (1983) and van Dijk et al. (2004) developed corrections to adjust sensible heat flux from sonic to actual air temperatures. An additional adjustment known as the crosswind correction (e.g. Liu et al., 2001) is also applied to the sensible heat flux. This correction accounts for the slightly longer path the acoustic pulse travels due to flow normal to the transducer path.

2.2.4 Anemometer models employed in this study

This study focuses on three models of sonic anemometers: the Gill R3 50 and Gill R3 100 both manufactured by Gill Instruments Ltd. (Lymington, UK) and the ATI Vx probe built by Applied Technologies Inc. (Longmont, CO). The two sets of instruments differ in their respective support structures and axis orientation (Fig. 2-3 to 2-6). The ATI Vx represents an example of a non-omnidirectional instrument, where the boom is oriented in the same horizontal plane as the measurement paths. Wind flowing from "behind" this instrument (over the mounting bar) should not be considered as high quality

data. The two Gill R3 models represent an omnidirectional design, with the support structure located below the measurement paths. The ATI Vx has the transducer sets oriented orthogonally while, in contrast, the Gill R3 anemometers have transducer sets oriented non-orthogonally. As noted for the Gill R3 units, a common configuration is that the measured axis wind velocities undergo an axis transformation so that the three orthogonal components of wind velocity (U, V, and W) are reported. In contrast, the output for the ATI Vx (Fig. 2.6) is not transformed to align with the mounting bar. Therefore, while W may be compared directly among anemometers, the U and V output, despite the same labels, cannot. This issue is resolved after double rotation is applied in the processing software. Multiple differences in configuration between the two sets of anemometers are detailed in Section 3. However, given the small differences between the Gill R3 50 and Gill R3 100 (e.g., maximum data stream output), we expect these two models of anemometers to behave very similarly in this comparison.

Figure 2-3. A photo of the Gill R3 100 omnidirectional ultrasonic anemometer manufactured by Gill Instruments, Ltd. (Gill R3 manual).

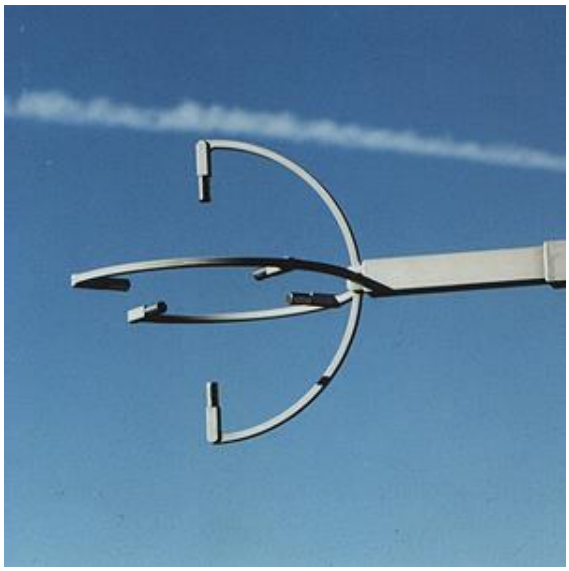

Figure 2-4. A photo of the ATI Vx Probe ultrasonic anemometer manufactured by Applied Technologies, Inc. (SATI S manual).

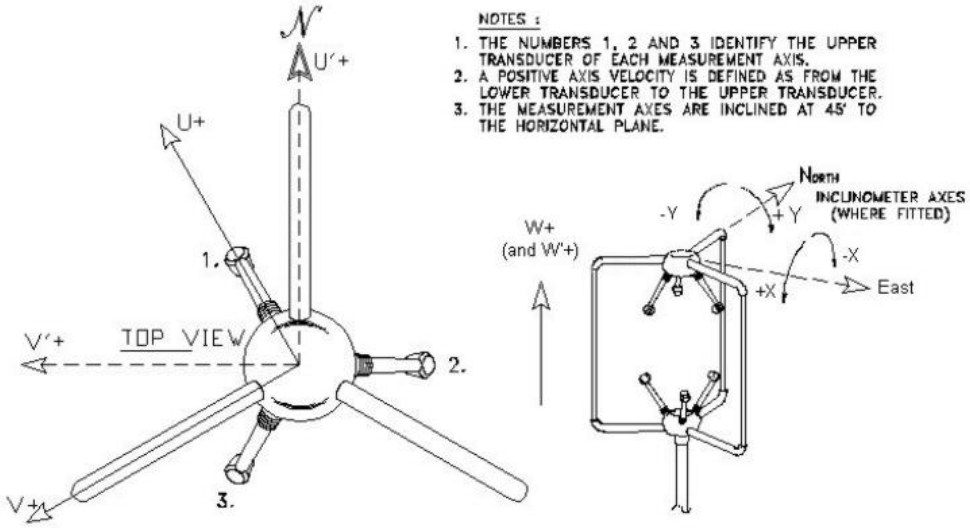

Figure 2-5. Schematic of the Gill model R3 100 and R3 50 axis orientation showing positive direction of U, V and W components. Note the U'+/V'+ orientation is used in this study (Gill R3 manual).

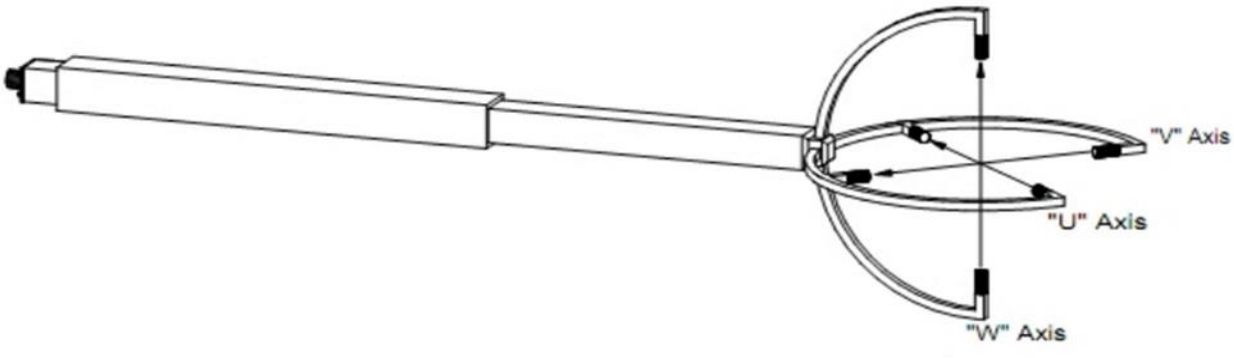

Figure 2-6. Schematic of the ATI Vx Probe axis orientation showing positive direction of u, v and w components. (SATI S Manual)

2.4 Angle of attack corrections for Gill sonic anemometers

Two procedures have been developed to correct for transducer flow distortion in the Gill R2/R3 and Gill Windmaster (Pro) omnidirectional sonic anemometers based on the angle of attack. Nakai et al. (2006) developed an algorithm for the R2/R3 anemometers that use a single 10Hz scan of U_o, V_o, and W_o (with subscript denoting observed values) and transforms these parameters into corrected values according to the following equations:

$$U = Uo * \frac{\cos(\alpha)}{fcr(\alpha,\gamma)} \quad \text{Eq. 2-12}$$

$$W = Wo * \frac{\sin(\alpha)}{fsr(\alpha,\gamma)} \quad \text{Eq. 2-13}$$

where α represents the angle of attack and γ represents wind direction expressed as:

$$\alpha = \arctan\left(\frac{Wo}{Uo}\right) \quad \text{Eq. 2-14}$$

$$\gamma = \left(180° - \arctan\left(\frac{Vo}{Uo}\right)\right) \quad \text{Eq. 2-15}$$

and the $f_{cr}(\alpha,\gamma)$ and $f_{sr}(\alpha,\gamma)$ functions correct for improper cosine and sine response due to flow distortion, respectively. The functions were derived from data collected in a wind tunnel from an older Gill model sonic (Gill R2) and the R3 model that had the same physical structure as the models in this study but older versions of firmware. The firmware has been improved for the newest Gill R3 models (T. Stickland, personal communications.). The Nakai and Shimoyama (2012) approach uses these same equations but with an "improved" polynomial expressions in $f_{cr}(\alpha,\gamma)$ and $f_{sr}(\alpha,\gamma)$. The Gill Windmaster Pro was used in the Nakai and Shimoyama 2012 study. The polynomials were also fit from data collected in turbulent flow over a short grass canopy. The magnitude of these corrections will depend on multiple factors including the measurement height above the surface/canopy and zero plane displacement, and roughness length. The correction ranged from 5% to 13% for H in three contrasting canopies as calculated in Nakai et al. (2006). Such corrections constitute the first manipulation performed to a single 10 Hz scan of uncorrected u_o, v_o, and w_o data. A corrected u, v, and w are generated for each corresponding u_o, v_o, and w_o.

Chapter 3. Materials and Methods

3.1 Site description and weather conditions

The field experiment was conducted at the US-Ne3 AmeriFlux site near Mead, NE (Size: 65 ha; Lat.: 41.1797˚ N; Long.: -96.4396˚ W; elev.: 363m). This rainfed site has been under strictly no-till management since 2001. The crops are rotated in alternate growing seasons between maize (*Zea mays*) and soybean (*Glycine max*). The field is very flat with sufficient fetch making it an ideal location to conduct these inter-comparison measurements. During the 2014 growing season, the field was planted in E-W rows with soybean (Fig 3-1) on May 19 (DOY 139). Planting density was 299,300 plants/ha. The crop emerged May 26 (DOY 146). The canopy height ranged from about 0.1 m before planting (i.e., corn stubble) to 0.88 m at the R5 growth stage (August 13; DOY 225) with peak green leaf area index of 3.7 m^2 m^{-2}. The canopy began to senesce and was harvested on October 8 (DOY 281). Remaining measurements through the fall/winter were made over soybean stubble (≈ .05 m).

Figure 3-1. Example of the E-W soybean rows (leaf area index ≈ 0.8 m^2 m^{-2}) at the study site.

Half hourly air temperature and relative humidity (measured at 3m) and an atmospheric pressure sensor on the AmeriFlux tower indicate a wide range in these quantities during the course of the study (Fig 3-2). These parameters were used to calculate ambient air density required for the calculation of fluxes. Even though these sensors were 50 m away from the tripod and measured at a slightly lower height, the impact on the results of this study would be minimal, while the potential flow distortion from an aspiration shield mounted on the tripod was eliminated. We note here and discussed below, mean sonic air temperature measured from the Gill R3 sensors is known to have a bias which does have a significant impact on flux magnitudes if those values are used to calculate air density. The prevailing wind direction at the site is from the south during the growing season in the summer and fall of 2014 (Fig. 3-2). There are also periods of higher wind speeds (> 8 m/s) from the northwest and north-northwest. Winds tend to be more from the north during the winter season but sufficient periods of good wind direction were obtained over the winter months (data not shown).

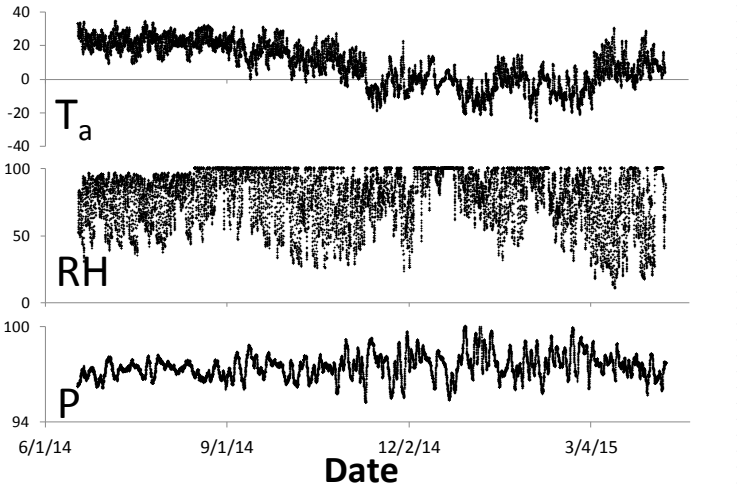

Figure 3-2. Distributions of air temperature (T_a, ^oC), relative humidity (RH, %), and air pressure (P, kPa) measured at the AmeriFlux tower US-Ne3 during the study.

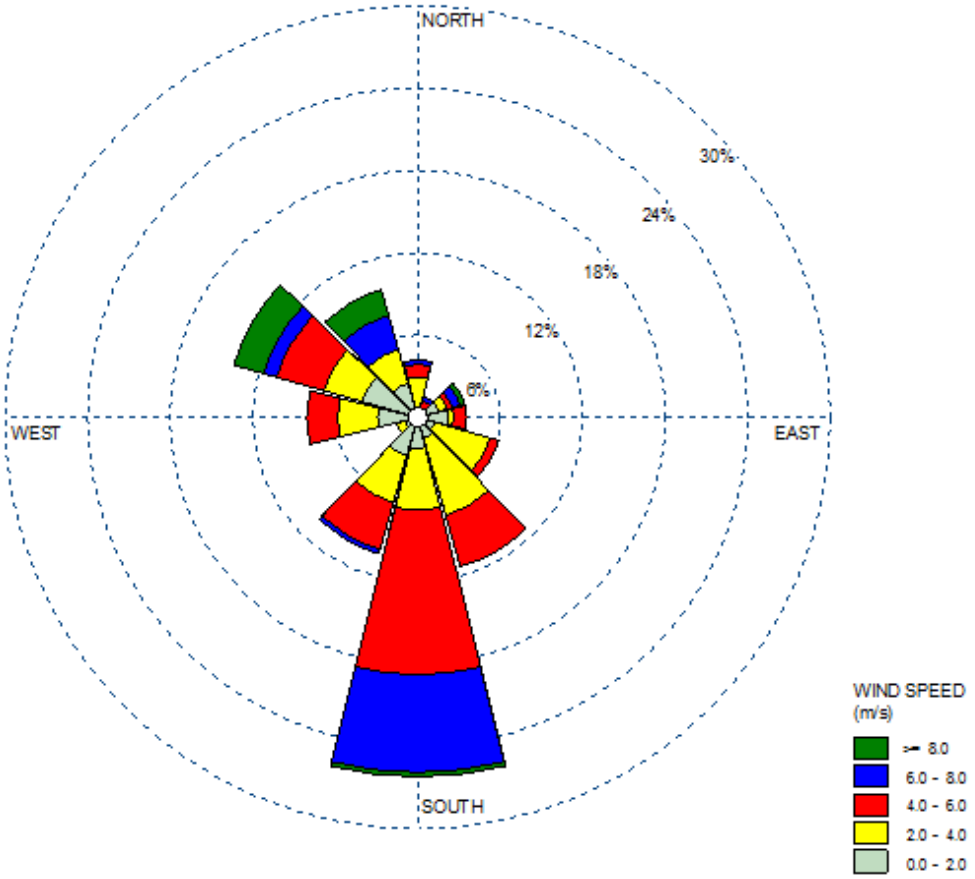

Figure 3-3. Wind rose for summer and fall 2014 (June 17 to October 3).

3.2 Instrument setup and configuration

A Gill R3 50, a Gill R3 100 (Gill Instruments Ltd., Lymington, UK) and an ATI Vx sonic anemometer (Applied Technologies Inc., Longmont, CO) were deployed on a tripod located 50 m directly west of the US-Ne3 AmeriFlux tower. A cross arm, supported at both ends, was installed to produce a measurement height of 4 meters above the ground. Given predominant wind directions, the ATI was deployed facing south and the Gill R3 anemometers were installed on either side of the ATI, separated by 0.75 m, with their north spar aligned with true north. Figure 3-4 includes two photos of the installation and a schematic representation of the anemometer arrangement (vertical

cones represent the limited wind directions that were used for the inter-comparison – see Section 3.5). Digital output from each anemometer was recorded at 10 Hz through three RS-232 ports on a CR3000 Micrologger (Campbell Scientific, Inc., Logan, UT) with a simple data collection program. The tripod was removed and reinstalled during planting and harvesting operations. Anemometers were leveled periodically during the experiment.

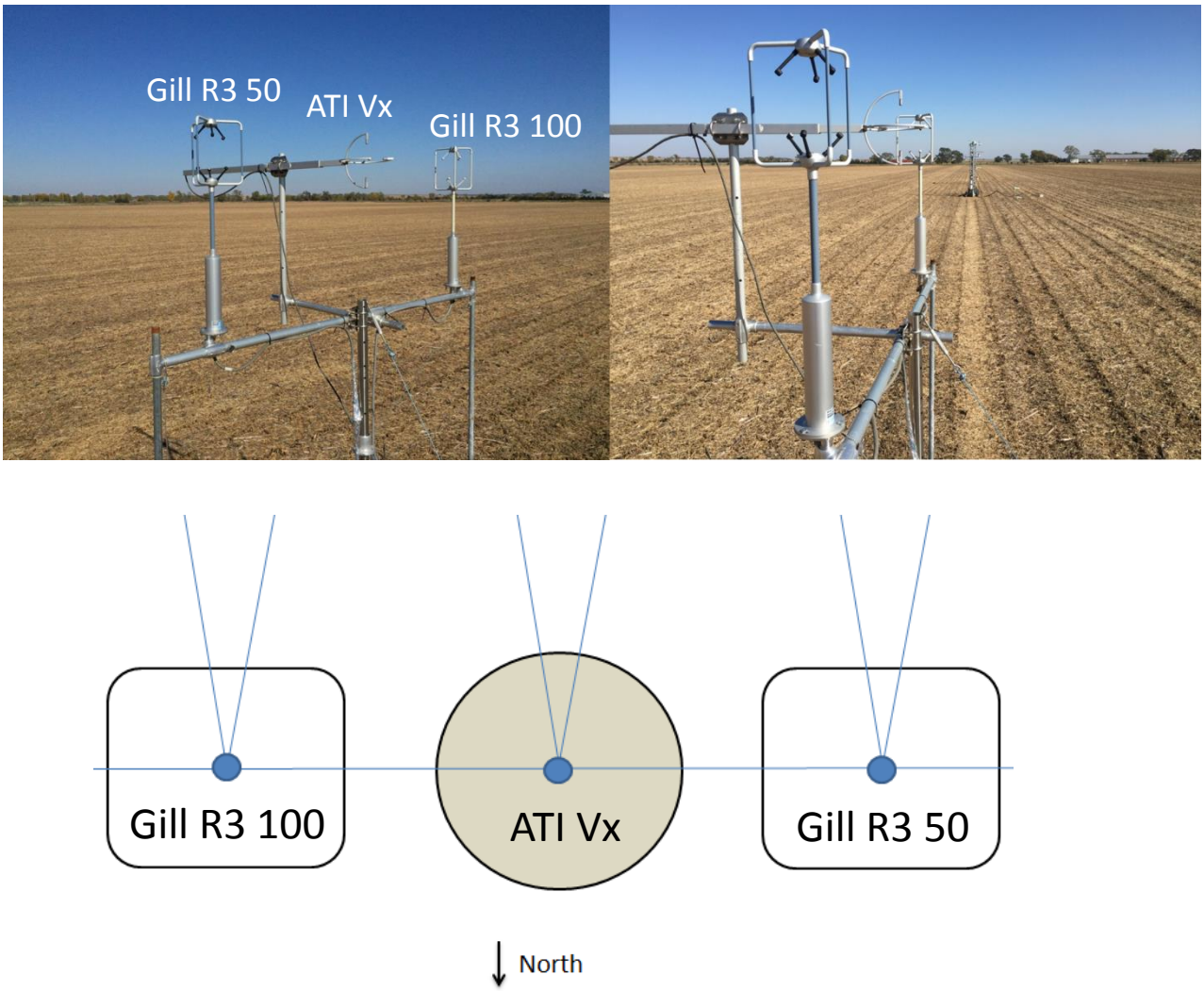

Figure 3-4. Photos of the sonic anemometer deployment (looking northeast and east). The schematic (view from above) includes the ranges of acceptable wind direction with instruments oriented south and separated by 0.75 m (Not to scale).

Each sonic anemometer had the most current version of the firmware (Table 3-1). For internal corrections, both Gill R3 anemometers were in the "UVW cal" mode meaning the non-orthogonal axis velocities are transformed via a coordinate transformation to a u-v-w (non-streamflow) coordinate system and a correction operation is applied to calibrate out the effects of the transducers and head framework. "Instantaneous mode" was off so there was internal averaging (100 or 50 Hz data is non-overlap-block averaged to 10 Hz output). A crosswind correction for sonic temperature measurement (Liu et al., 2001) was applied via firmware using a composite of the three non-orthogonal axis velocities. For the ATI, internal sampling was set at 200 Hz with 20 samples (non-overlap-block averaged) to have 10 Hz output. A shadow correction was applied following Kaimal (1990) and the crosswind correction was generated using only the vertical velocity axis, in contrast to the Gill procedure.

Table 3-1. Configuration metadata for the Gill R3 50, Gill R3 100 (Gill Instruments Ltd.) and ATI Vx (Applied Technologies) sonic anemometers. Manufacture/calibration date and firmware version for the ATI probe is unknown.

Sonic Brand	Gill Instruments	Gill Instruments	Applied Technologies
Model	R3 50	R3 100	Vx Probe
Serial # / Firmware	494 / v. 3.01	499 / v 3.01	120804 / unknown
Transducer Orientation	Non-orthogonal	Non-orthogonal	Orthogonal
Internal Corrections	Enabled	Enabled	Enabled
Manufacture Date	November, 2010	March, 2011	Unknown
Calibration Date	November, 2010	March, 2011	Unknown

3.3 Eddy covariance data processing and screening

EddyPro® Software (v6.0; LI-COR Biosciences, Lincoln, NE) processed the anemometer *u*, *v*, *w*, and *Ts* 10Hz data into 30 minute fluxes for each sonic anemometer.

Table 3-2 documents the metadata. Block averaging, axis rotation, and despiking procedures were identical among the anemometers. Frequency response corrections (following Moncrieff et al., 1997) effectively corrected only for path length averaging, since sensor separation, time response, and time delay are not relevant factors for themeasurements of sensible heat flux and friction velocity. Note the angle of attack corrections were not applied when making initial comparisons between sonic anemometers but were selected when reprocessing these datasets a second and third time (see Section 4.3) to quantify the magnitude of these corrections.

Wind direction and a turbulent stationarity scale formed the basis for quality assurance and quality control of the 30 minute fluxes. Fluxes were selected for periods having mean rotated horizontal wind directions from 180°±20° to minimize the influence of flow distortion from adjacent anemometers and support structures. Fluxes were also selected for periods of steady-state conditions following Foken and Mauder (2004). Only fluxes flagged with a 0 (on the 0-1-2 scale for stationarity) were selected. As the fluxes were calculated independently among sensors, the screening procedure resulted in a slightly different number of half hour fluxes that were used in this analysis (1219, 1331, and 1389 half hour fluxes for the ATI Vx, Gill R3 50 and Gill R3 100, respectively).

Table 3-2. Eddy covariance processing metadata for the Gill R3 and ATI sonic anemometers.

	Gill R3 50/Gill R3 100/ATI Vx
Averaging	Block
Axis Rotation	Double ($\bar{W}$=0, $\bar{V}$=0)
Despiking	Vickers and Mahrt (1997)
Frequency Response Correction	Applied in EddyPro® following Moncrieff et al. (1997) with minimal impact due to sensor separation/time response/time delay
QA/QC	Stationarity from Mauder and Foken (2004) as applied in EddyPro®, Wind Direction from 180^{o}±20°
Supporting Data	US-Ne3 T/RH/P measured at 3m height 50 m away

Chapter 4 Results and Discussion

4.1 Baseline Sonic Comparison

4.1.1 Evaluation of unprocessed 10 Hz data

The pitch angle (angle between the u-v plane of the instrument and the plane of horizontal streamflow derived from coordinate rotation) is shown in Figure 4-1 for each anemometer for all hours of data as a function of wind direction. From the range of 180^{o} ± 20^{o}, the pitch angle for each anemometer is generally within about ±2°. As the wind shifts, the pitch shows more scatter possibly due to flow interference among the sensors. For example, for the ATI Vx probe, there is more variability in the pitch angle for winds from 90^{o} and 270^{o} where the wind is blowing through a Gill sonic. The Gill R3 100, mounted on the east side of the array, shows the largest pitch angle for winds around 270^{o} where the wind blows through the Gill R3 50 and mounting structure of the ATI Vx probe. These results suggest flow interference among anemometers was minimized for our range of acceptable wind directions.

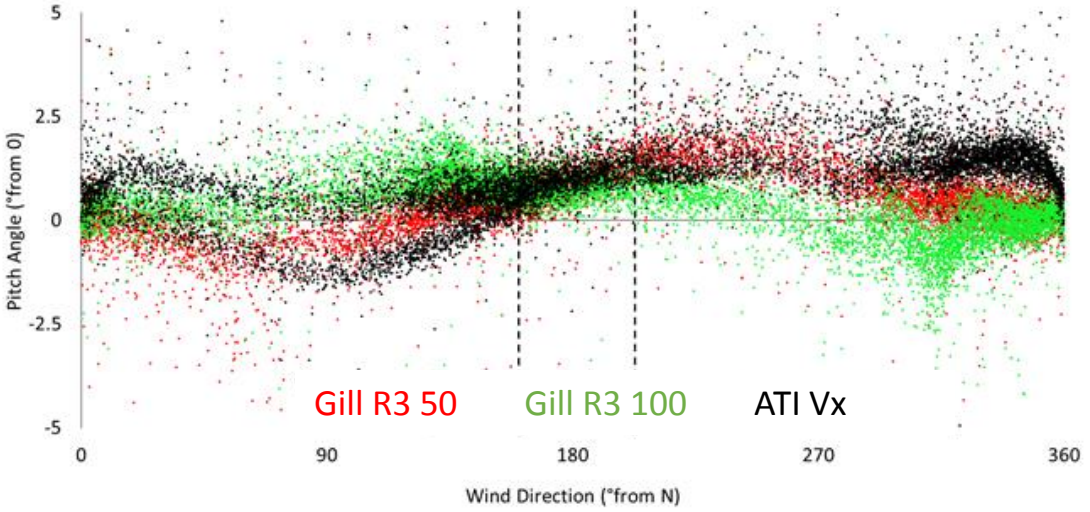

Figure 4-1. Pitch angle of each sonic anemometer as a function of wind direction for all data collected during the measurement period (dashed lines indicate 180^{o}±20^{o} range).

A half hour samples of the 10 Hz horizontal and vertical wind speeds and sonic temperatures meeting the screening criteria from each anemometer are compared in Figure 4-2. In general, the distribution of horizontal wind speed among the three sonic anemometers seems to compare reasonably well. A 1:1 comparison of these data (Figure 4-3) show generally good agreement with some scatter between values of horizontal velocity. We note, as also was done in Frank et al. (2013), the analysis in this study is not based on the assumption that the three sonic anemometers measure the same wind vector. Rather, we expect the turbulent statistics among the anemometers (including fluxes) to agree well in the absence of non-orthogonal flow distortion. We further note the sonic temperature comparison reflects the known offset in the Gill R3 sonic temperature measurements. This offset is an artifact of the design/material used to protect the transducers (T. Stickland, Gill Instruments Ltd., personal communication). The presence of this material causes a slight additional delay in the sonic T measurement that leads to an offset. This offset is sensitive to the temperature of the material so the offset varies for large changes in temperature. However, for short time periods (half hour), this delay is constant and mostly cancels when determining sonic air temperature fluctuations. Figure 4-2 indicates this offset may be different for different anemometers. The offset in mean temperature may be large enough that it will bias calculations of air density used in calculating sensible heat flux and friction velocity. So, an independent measurement of mean temperature should be collected when using the Gill sonic anemometer.

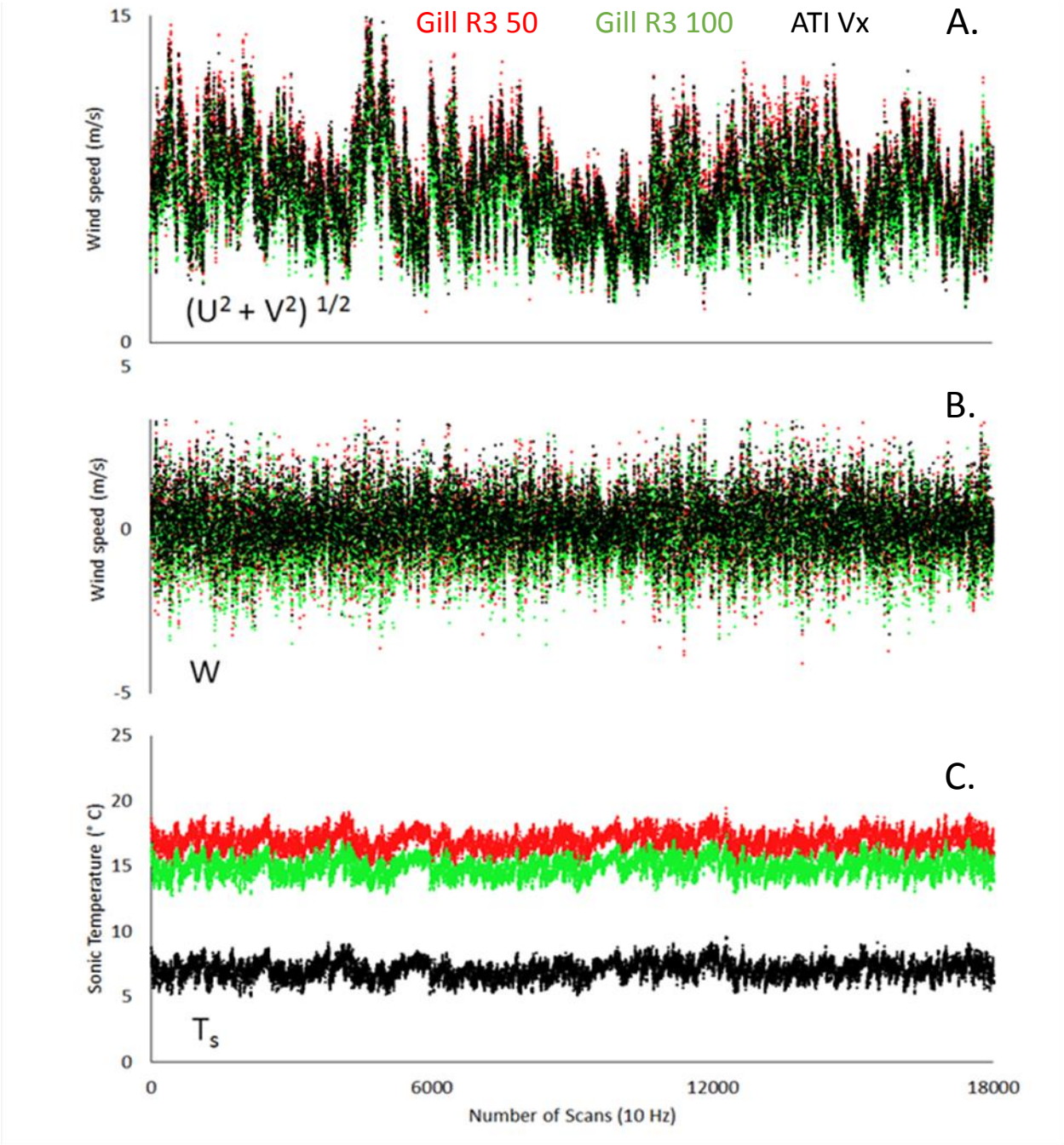

Figure 4-2. One half hour of A) horizontal windspeed, B) vertical windspeed and C) sonic temperature recorded at 10 Hz for the three anemometers Gill R3 50, Gill R3 100, and the ATI Vx (note 10 scans = 1 sec).

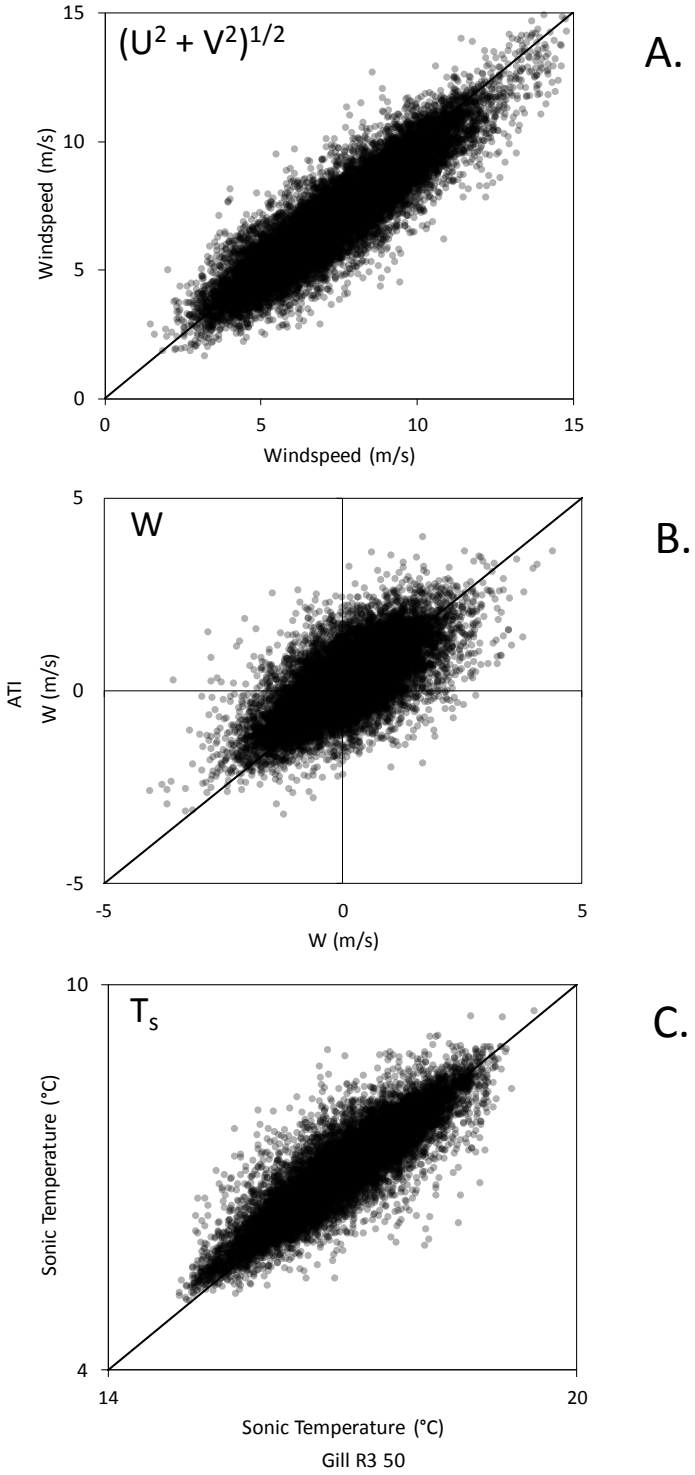

Figure 4-3. Comparison of A) horizontal, B) vertical, and C) sonic temperature measurements from ATI Vx versus Gill R3 50 over one half hour (same data as Fig 4.2). Data points represent "unprocessed" values as output by the instrument. The 1:1 line is shown in each panel.

4.1.2 Evaluation of Processed Mean Quantities

A comparison of 30 minute mean, rotated, horizontal wind speed (U) and sonic temperature (T_s) among anemometers is presented below. All data met the screening criteria and no angle of attack corrections have been applied. Among all anemometers, there is very little scatter in the U data ($R^2 > 0.999$; Fig 4-4). However, Gill R3 50 overestimates U by 4% and Gill R3 100 overestimates U by 2% compared to the ATI Vx, respectively. For sonic temperature (T_s), the scatter is only slightly worse ($0.96 < R^2 < 0.98$; Fig 4-5). However, there is a significant bias (18-20 K) between the Gills and ATI Vx, and less than a 1K bias between Gill models. Furthermore, the slope of the temperature relationship between the ATI and Gills is considerably less than one, but this may be a function of the relationship at colder ambient temperatures (<280 K). The non-linear nature of the relationship between the ATI Vx and Gill R3 is likely due to the temperature-dependent offset as previously noted (see Fig. 4-2).

4.2 Evaluation of non-orthogonal flow distortion

4.2.1 Standard deviations

The standard deviation of the orthogonal wind components provides a statistical representation of the variability of the wind component measured by the contrasting anemometer designs. The two Gill sonic anemometers overestimate σ_u compared to the ATI Vx by about 3 - 5% (Fig. 4-6). In contrast, σ_v and σ_w are underestimated by about 3-5% (Figs. 4-7 and 4-8). Between Gills, there is also a slight difference (1-2%) with the Gill R3 50 having the slightly larger values. As the case for mean windspeed, the R^2 in each relationship is very high (0.988 to 0.999).

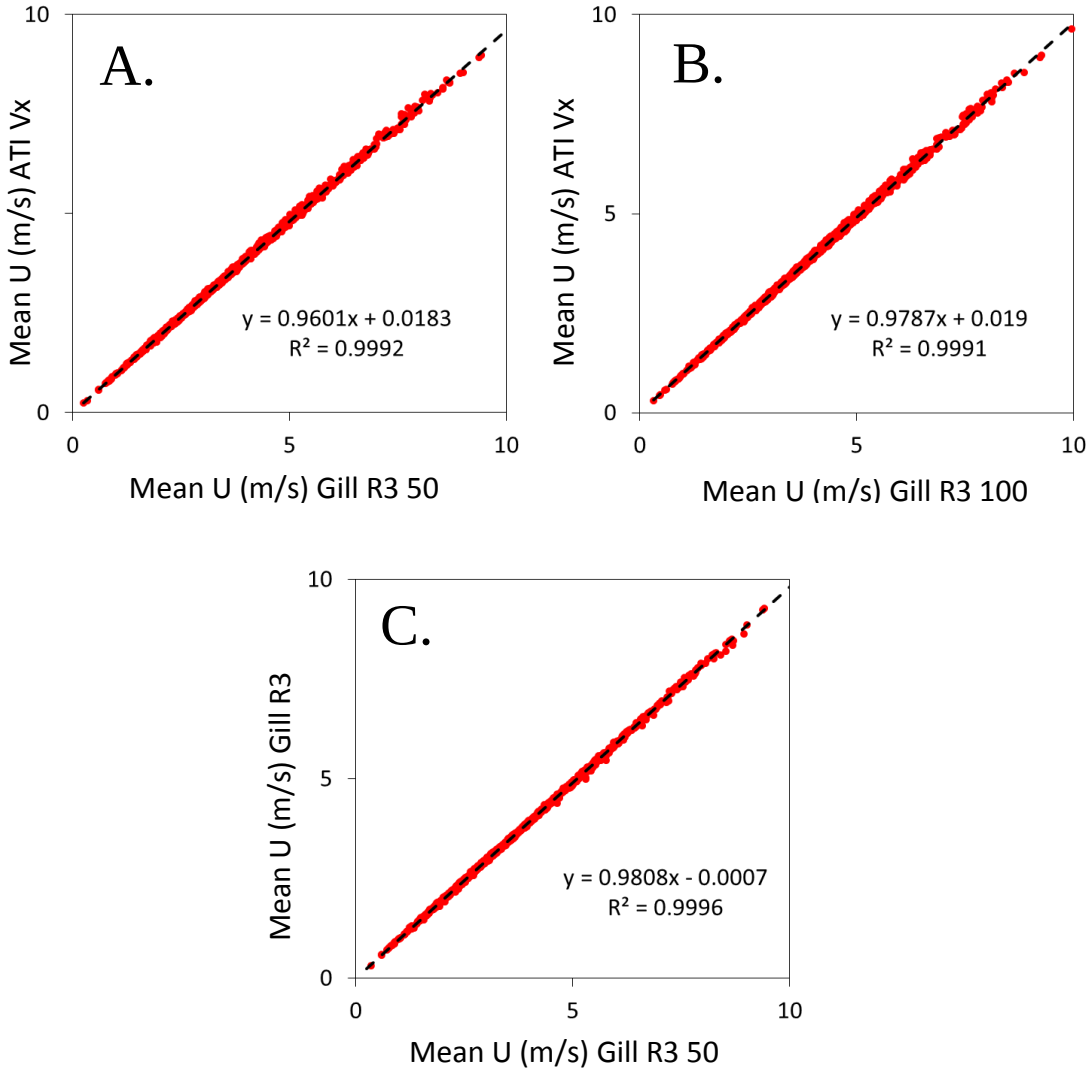

Figure 4-4. Comparison of processed mean horizontal wind speed (U) between A) ATI Vx and Gill R3 50, B) ATI Vx and Gill R3 100, and C) Gill R3 100 and Gill R3 50.

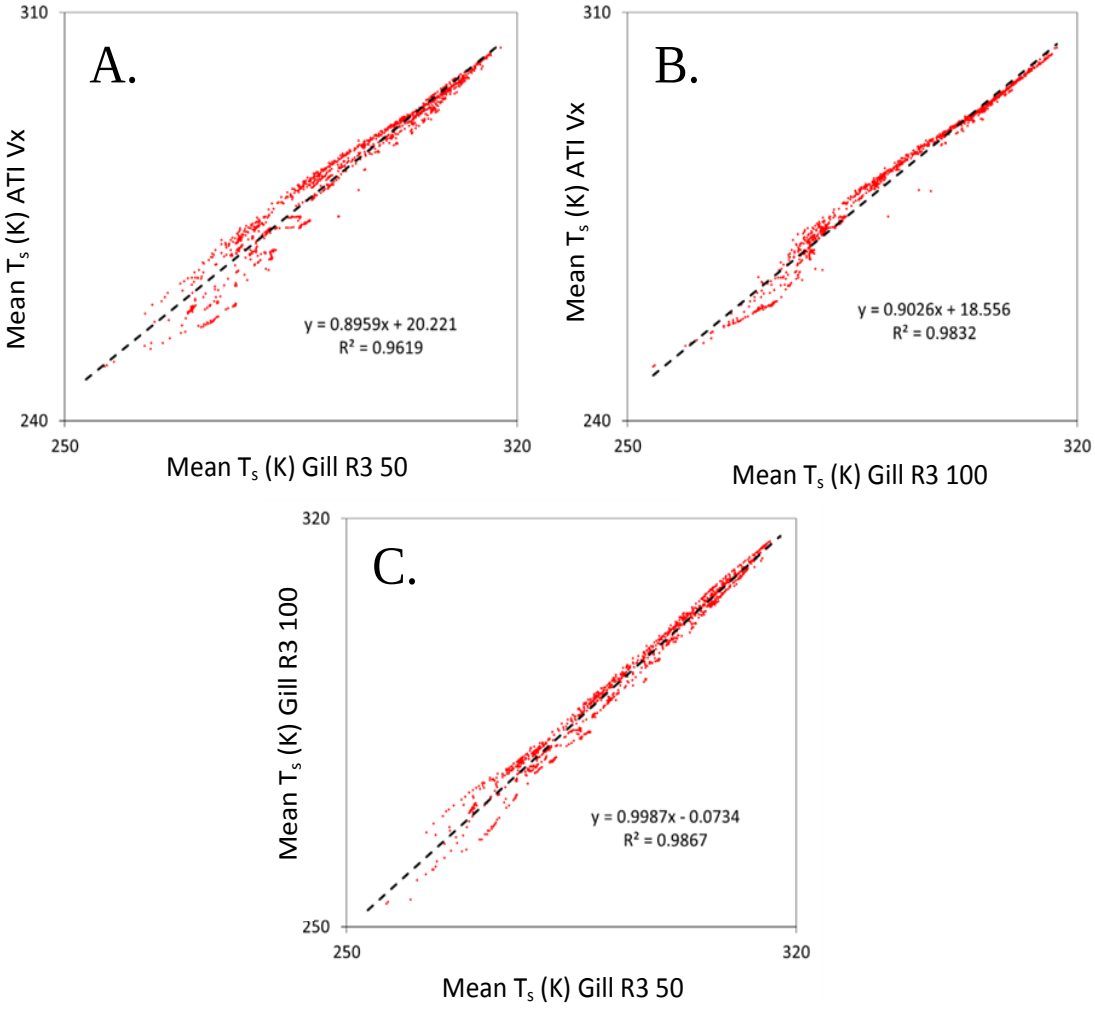

Figure 4-5. Comparison of mean sonic temperature (mean T_s) between A) ATI Vx and Gill R3 50, B) ATI Vx and Gill R3 100, and C) Gill R3 100 and Gill R3 50.

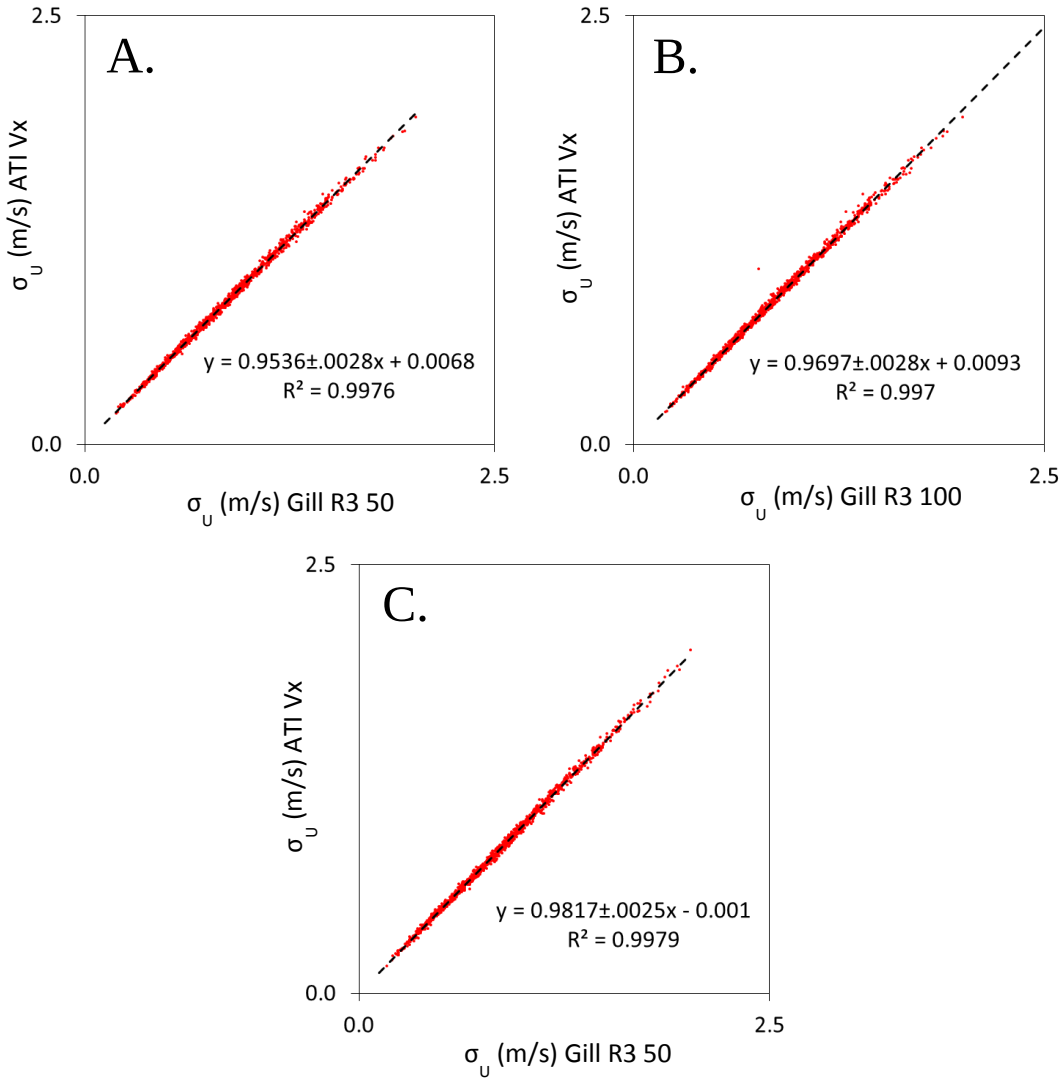

Figure 4-6. Comparison of the standard deviation of the horizontal component of wind speed (σ_u) between A) ATI Vx and Gill R3 50, B) ATI Vx and Gill R3 100, and C) Gill R3 100 and Gill R3 50. Data have been screened and no angle of attack corrections have been applied. The slope includes a 95% confidence interval determined using R linear model analysis.

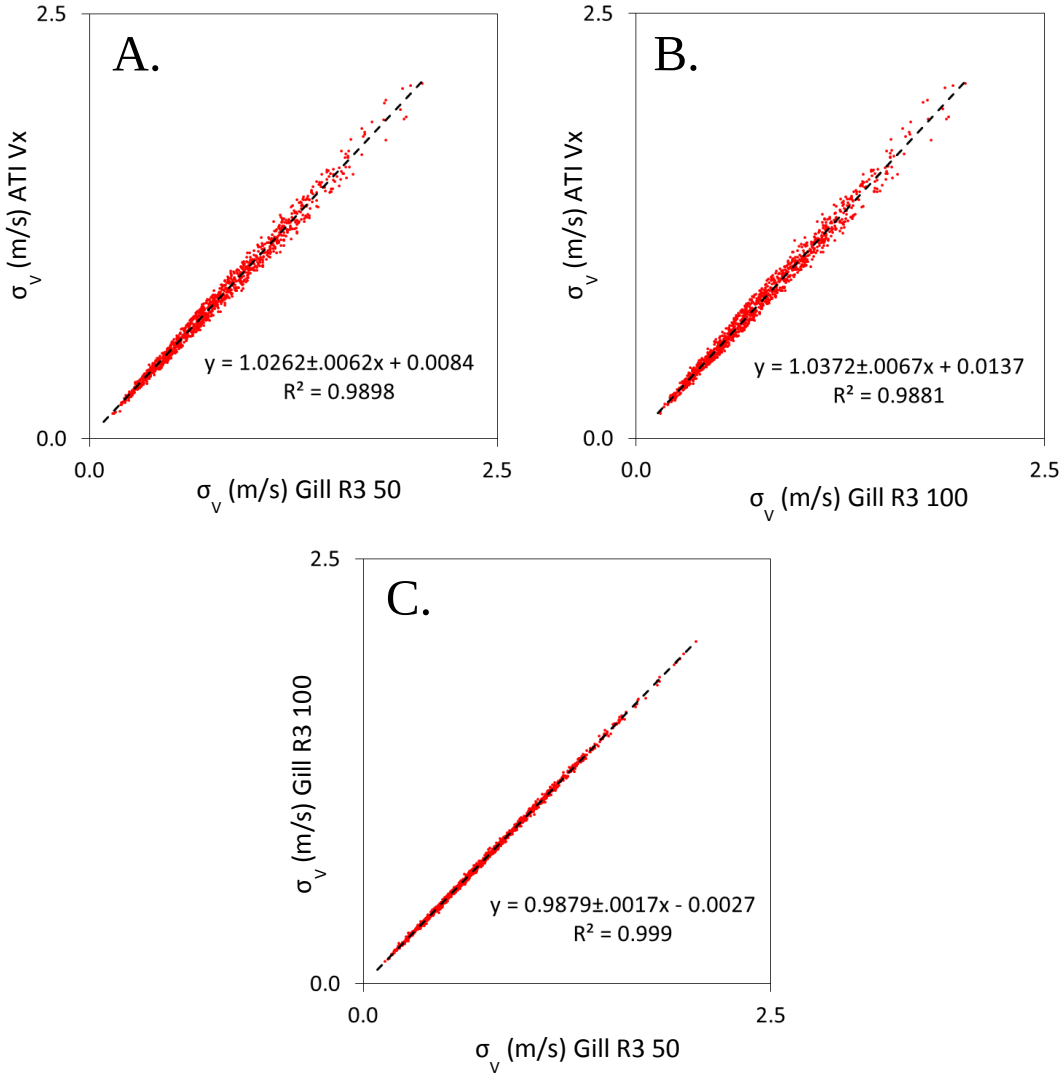

Figure 4-7. Same as Figure 4-6 for the standard deviation of the (rotated) crosswind component of wind speed (σ_v).

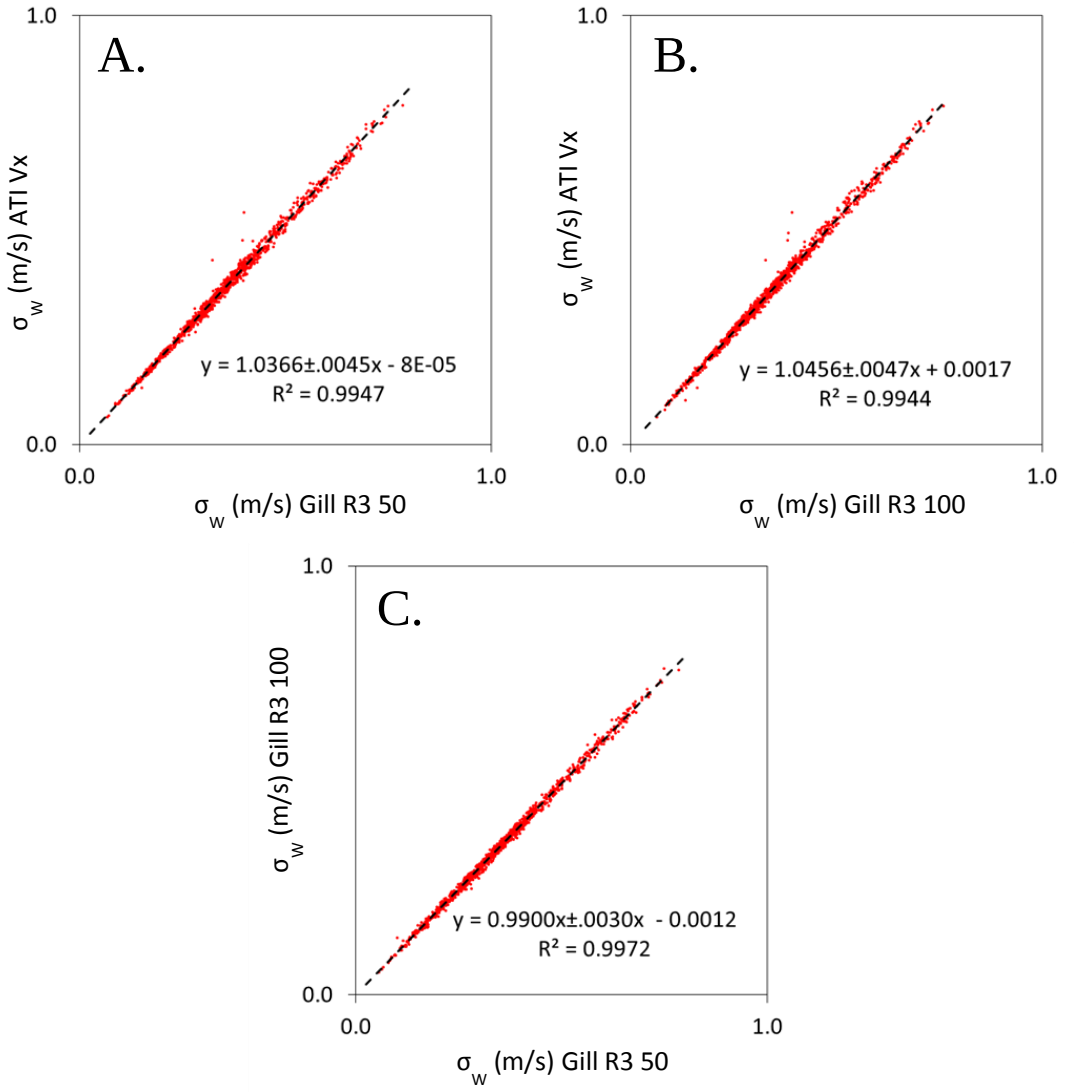

Figure 4-8. Same as Figure 4-6 for the standard deviation of the vertical component of wind speed (σ_w).

There is considerably more variability in sonic temperature (σ_{Ts}) comparisons. The R^2 varies from 0.76 to 0.83 between the Gills and ATI Vx but increases to 0.95 between the two Gills (Fig. 4-9). It is not fully clear if flow distortion in the Gills would impact the determination of sonic temperatue, although data in Section 4.4.1 suggests there may be a small impact. The σ_{Ts} for the Gills shows they are higher by 13% compared to the ATI (and only about 3% difference between Gills).

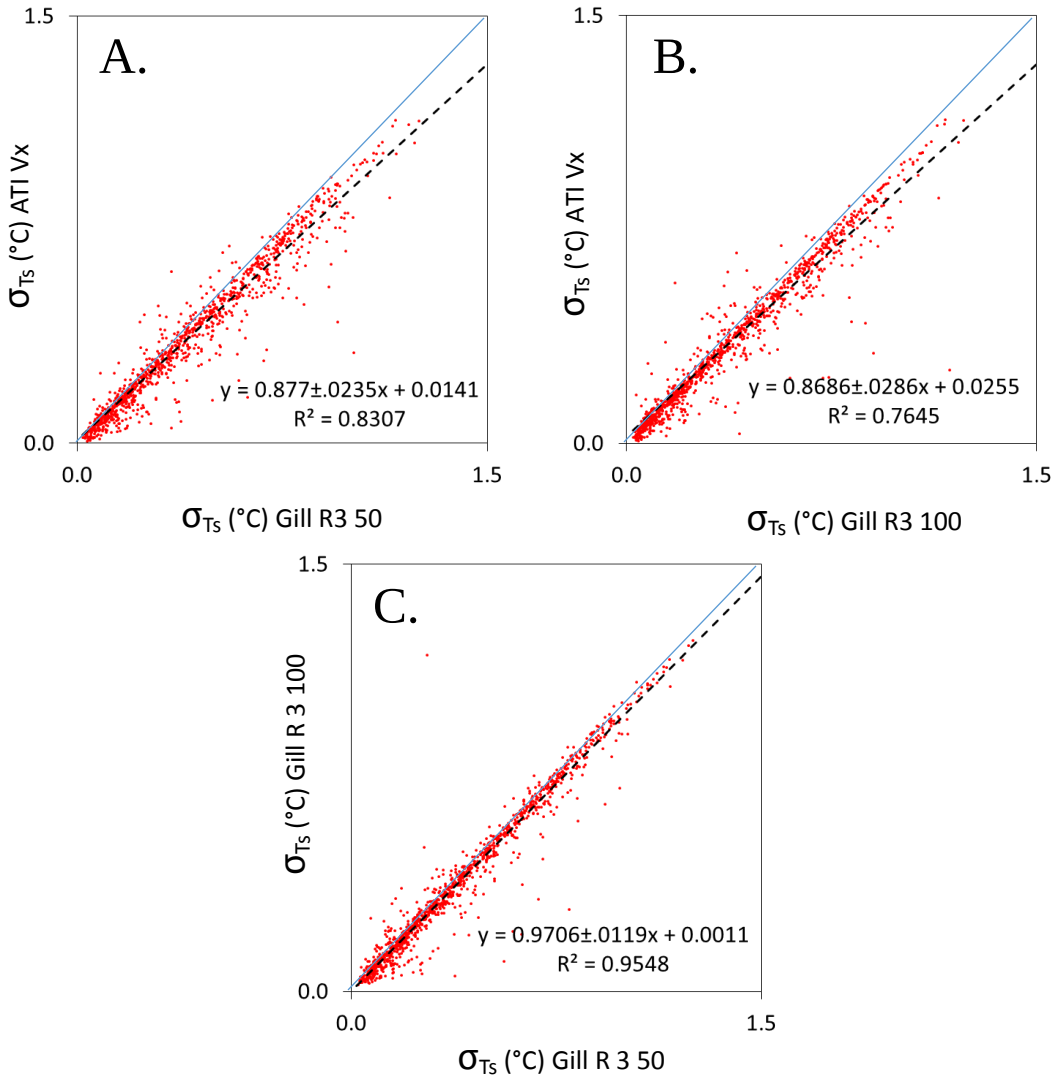

Figure 4-9. Same as Figure 4-6 for the standard deviation of sonic temperature (σ_{Ts}). A 1:1 line is included.

4.2.2 Sensible heat flux

The seasonal distribution of sensible heat fluxes (H; Fig. 4-10) during the measurement period ranged from about -100 to +375 W m^{-2} (flux away from the surface is positive). Even during the coldest months, we measured H on some days as large as 200 W m^{-2}. We note no angle of attack corrections were applied to the Gill sonic

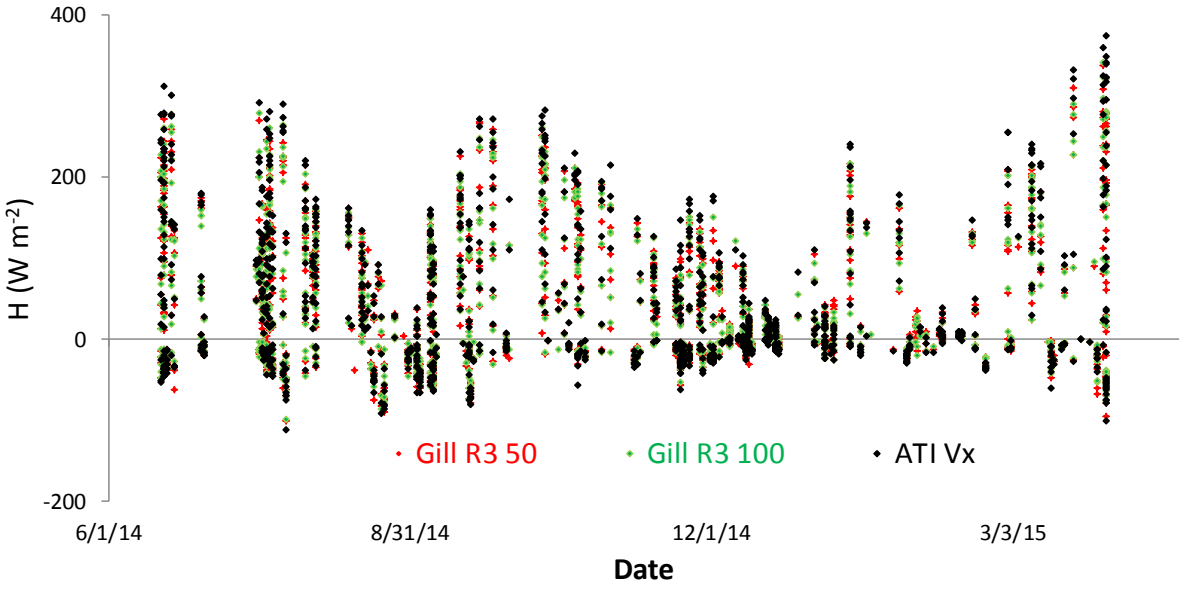

Figure 4-10. Sensible heat flux (*H*) time series for the time period June, 2014 to April, 2015. Data gaps represent filtering of half hourly averaging periods to remove periods of non-stationarity and wind direction outside of 180˚ ± 20˚ as measured by each instrument (see Sec. 3.3 for details). No angle of attack corrections have been applied.

anemometer H fluxes. The two Gill sonic anemometer models compared very well, with slope of 0.99 and correlation coefficient of 0.99 (Fig. 4-11). The Gill R3 50 and Gill R3 100 sensible heat fluxes compared to the ATI Vx also had very high correlation (R^2 > 0.99). However, the Gill sonic anemometers underestimated the sensible heat flux by about 12% (note the slope of the relationship, where H from the ATI Vx would be considered as the "independent variable" and plotted on the y-axis, is the Gill R3 correction factor). This supports the hypothesis that sensible heat flux magnitudes are impacted when using the non-orthogonal design (Gill R3 omnidirectional) compared to the orthogonal design (ATI Vx probe). We note as a result of the high correlations coefficients and intercepts essentially zero, a correction factor may be applied to non-orthogonal fluxes as a good approximation to the impact of non-orthogonal flow distortion.

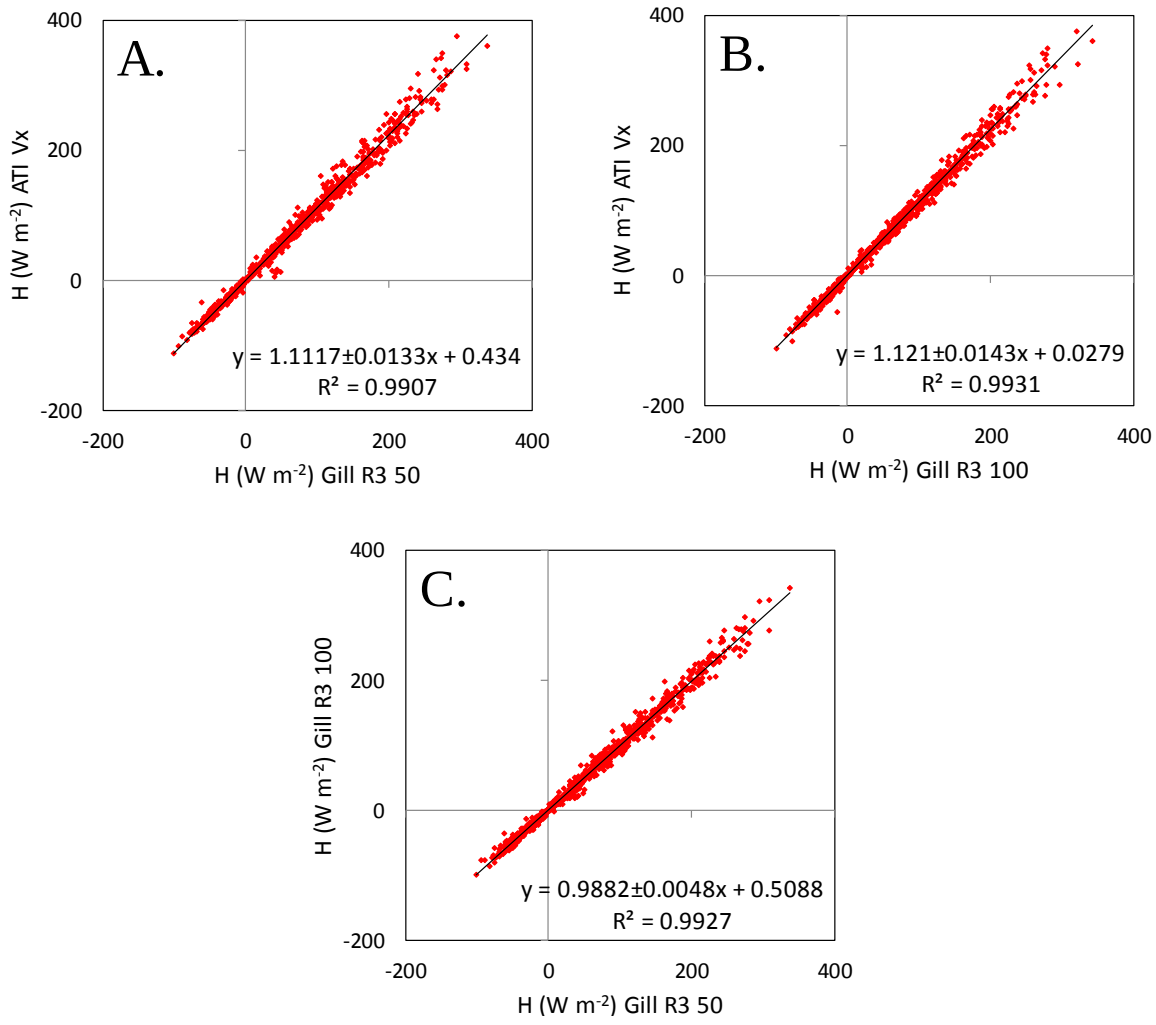

Figure 4-11. One to one comparison of sensible heat fluxes (H) between A) ATI Vx and Gill R3 50, B) ATI Vx and Gill R3 100, and C) Gill R3 100 and Gill R3 50. Data have been screened and no angle of attack corrections have been applied. The slope includes the 95% confidence interval determined using R linear model analysis.

4.2.3 Friction velocity

Figure 4-12 shows friction velocity (u_*) for the time period June, 2014 to April, 2015. Values range from 0.02 to 0.76 m s^{-1}. No angle of attack corrections have been applied to u_*.

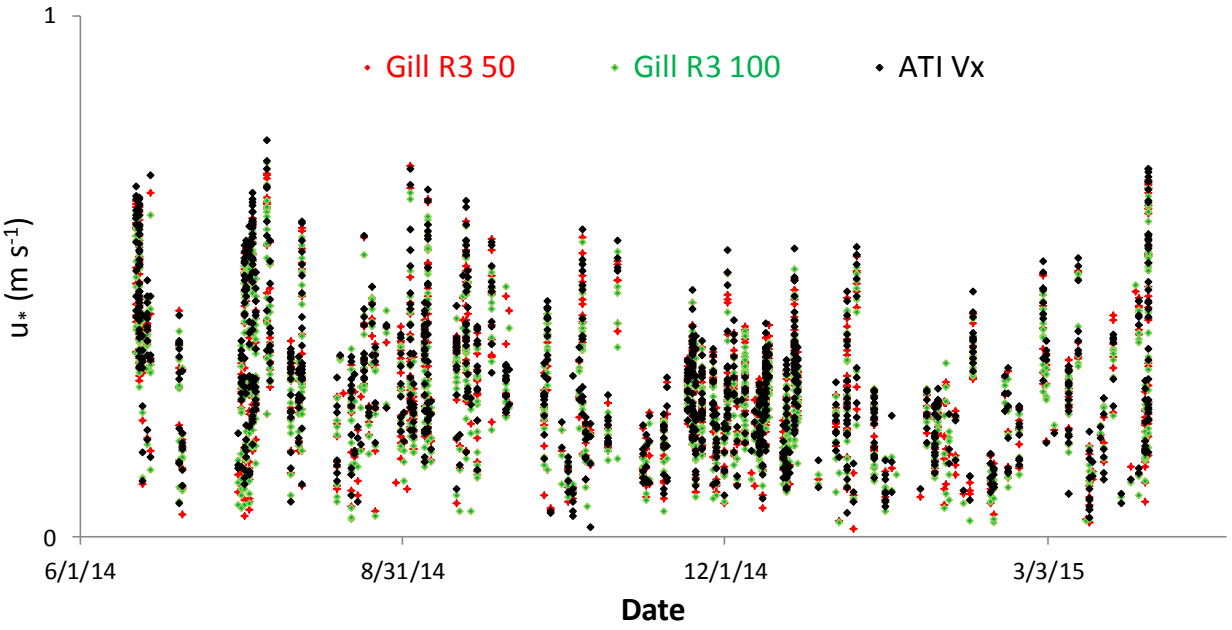

Figure 4-12. Friction velocity (u_*) time series for the time period June, 2014 to April, 2015. Data gaps represent filtering of half hourly averaging periods to remove periods with non-stationarity and wind direction outside of 180˚ ±20˚ as measured by each instrument (see Sec. 3.3 for details). No angle of attack corrections have been applied.

A 1:1 comparison between Gill R3 100 and Gill R3 50 friction velocity shows a slight difference between anemometers (slope of 0.97; Fig 4-13). Both Gill sonic anemometers underestimate friction velocity compared to the ATI Vx by about 3 to 5%. Correlation coefficients are greater than 0.98 for all comparisons. These results demonstrate the underestimation in friction velocity is considerably smaller than that for the sensible heat flux as summarized in Table 4-1. This phenomenon would be consistent with some of the flow from one axis (i.e., w) being distorted to another axis (i.e., u) due to interruption of flow by transducer and transducer support structure. This distortion may also be a result of coordinate transformations applied internally (Eqn. 2-6 to 2-8). As friction velocity uses two of the transformed axes, the flow distortion may be partially offset.

This would not happen for sensible heat flux which only uses the vertical velocity. We note Nakai et al. (2014) and Kochendorfer et al. (2012) also the underestimation of friction velocity to be smaller compared to sensible heat flux.

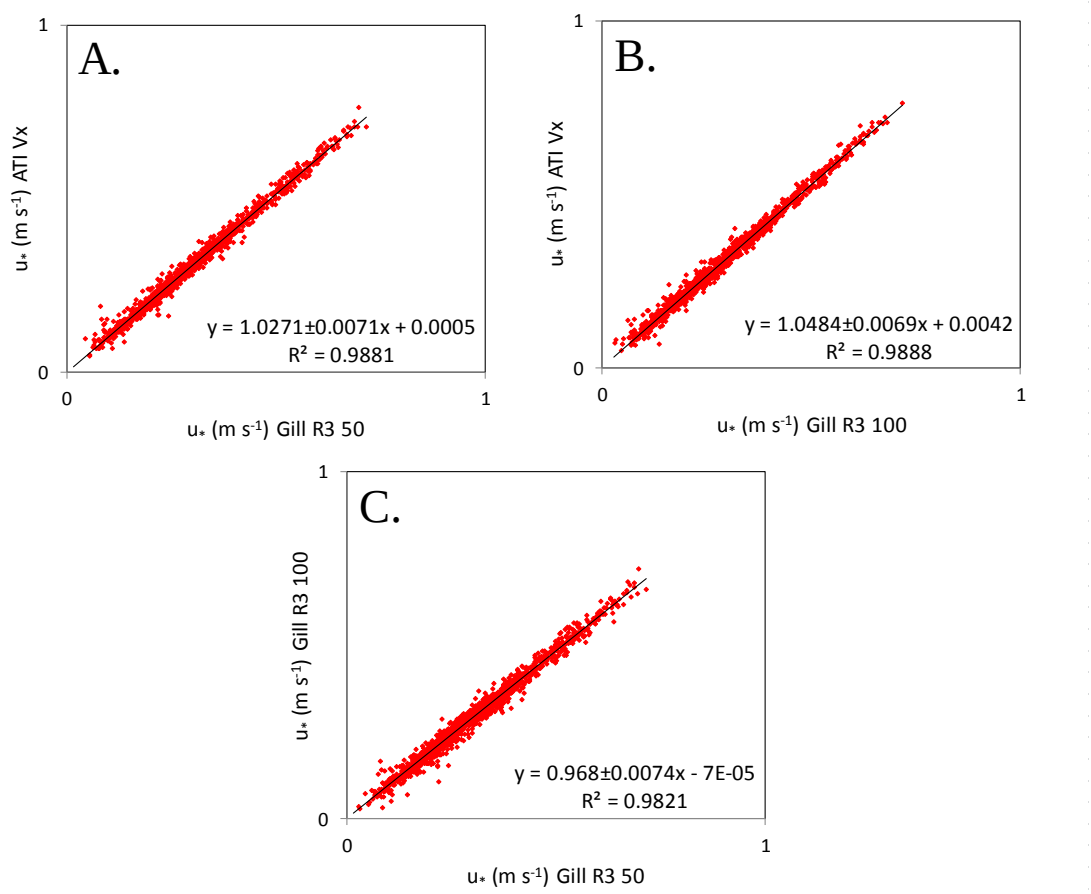

Figure 4-13. One to one comparison of friction velocity (u_*) between A) ATI Vx and Gill R3 50, B) ATI Vx and Gill R3 100, and C) Gill R3 100 and Gill R3 50. Data have been screened and no angle of attack corrections have been applied. The slope includes the 95% confidence interval determined using R linear model analysis.

When compiled together with the underlying assumption that flow distortion is minimal for the orthogonal ATI Vx probe, the results indicate clear underestimation of the fluxes for the non-orthogonal anemometer. The vertical velocity is being underestimated which subsequently affects the sensible heat flux and friction velocity. These results are consistent with previous studies of non-orthogonal anemometers with expected variations in the magnitude of the underestimation for reasons already noted (Sec. 1.1). This study has quantified the field- measured underestimation of H and u_* for this particular model of Gill sonic with current versions of firmware. Previous to this study at the US-Ne1, US-Ne2, and US-Ne3 AmeriFlux sites, modeled corrections were employed (Nakai et al., 2006) without field data from orthogonal anemometer to verify the accuracy of the correction. From these data, we may now verify the accuracy of the angle of attack corrections.

Table 4-1 Gill R3 (50 and 100) and ATI Vx slope coefficients for linear regression analysis. The table shows the slope of a linear regression of ATI Vx values plotted against Gill R3 values. A number greater than 1 indicates ATI Vx values are higher in magnitude than those of the Gill R3. A number below 1 indicates that the ATI Vx values are lower in magnitude than those of the Gill R3.

			ATI Vx				
			H	u_*	σ_u	σ_v	σ_w
Gill R3	H	R3 50	1.11				
		R3 100	1.12				
	u_*	R3 50		1.03			
		R3 100		1.05			
	σ_u	R3 50			0.95		
		R3 100			0.97		
	σ_v	R3 50				1.03	
		R3 100				1.04	
	σ_w	R3 50					1.04
		R3 100					1.05

4.3 Angle of attack corrections

As noted above, by this point in our analyses, no angle of attack corrections were applied to the processed fluxes/turbulent statistics for the Gill R3 or ATI anemometers. There are two options for angle of attack corrections using EddyPro® processing software: the Nakai et al. (2006), and Nakai and Shimoyama (2012) here after referred to as N2006 and NS2012, respectively. Data from June 17 to October 2, 2014 were reprocessed second and third time with no other changes except selecting each of these angle of attack options for the Gill R3 anemometers. We first evaluated the impact of each angle of attack correction on the fluxes (Fig. 4-14). Only data from the Gill R3 50 is shown as results were virtually identical for the R3 100. The NS2006 correction increased fluxes by 5% and the NS2012 correction by 16%. The corresponding corrections for friction velocity were 4% and 8%, respectively. When the angle of attack corrected fluxes are compared (Fig. 4-15; only Gill R3 50 shown), in general, the N2006 correction continues to underestimate the fluxes while the NS2012 correction overestimates the fluxes (regression slopes less than 1). For the N2006 procedure, data used in this analysis were obtained from wind tunnel measurements and older versions of firmware were used. For the NS2012, data were obtained from a field study and improved functions were incorporated. However, at the time of writing, we became aware of an issue that may have affected NS2012 analysis. An adjustment factor known as "w boost" may not have been applied in the Windmaster Pro anemometers used in that study. If it wasn't, the correction procedure would likely have incorporated this error and generated a larger correction factor. This issue is currently being explored. For now, it

seems neither correction factor is accurately capturing the non-orthogonal flow distortion observed in the present Gill R3 sonic anemometers.

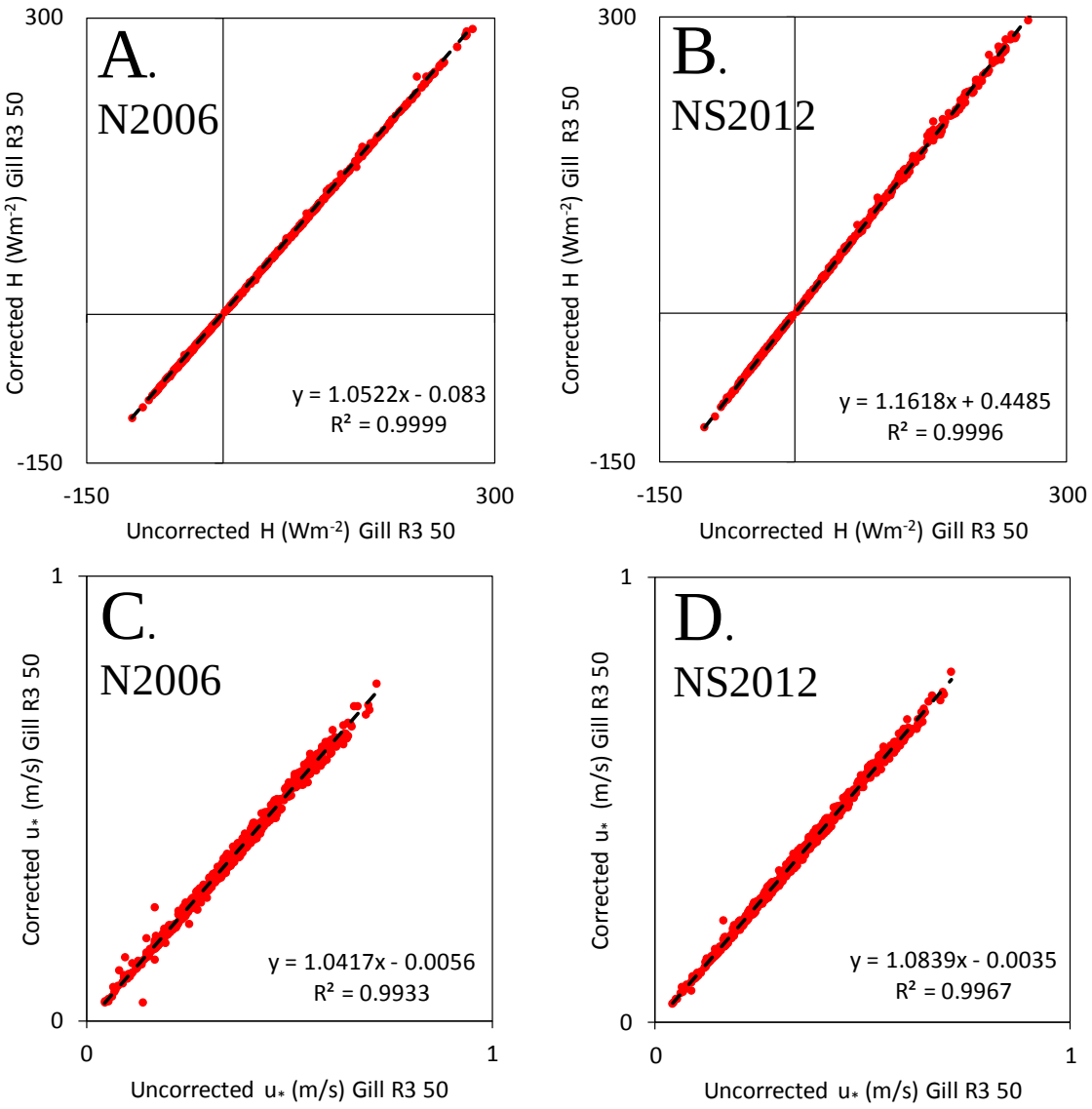

Figure 4-14. Comparison of uncorrected and angle of attack corrected fluxes for the Gill R3 50 anemometer for A) sensible heat flux (H) with the N2006 correction, B) sensible heat flux with the NS2012 correction, C) friction velocity (u*) with the N2006 correction, and D) friction velocity with the NS2012 correction. Data are from June 17th to October 2nd, 2014. See text for details on the N2006 and NS2012 angle of attack corrections.

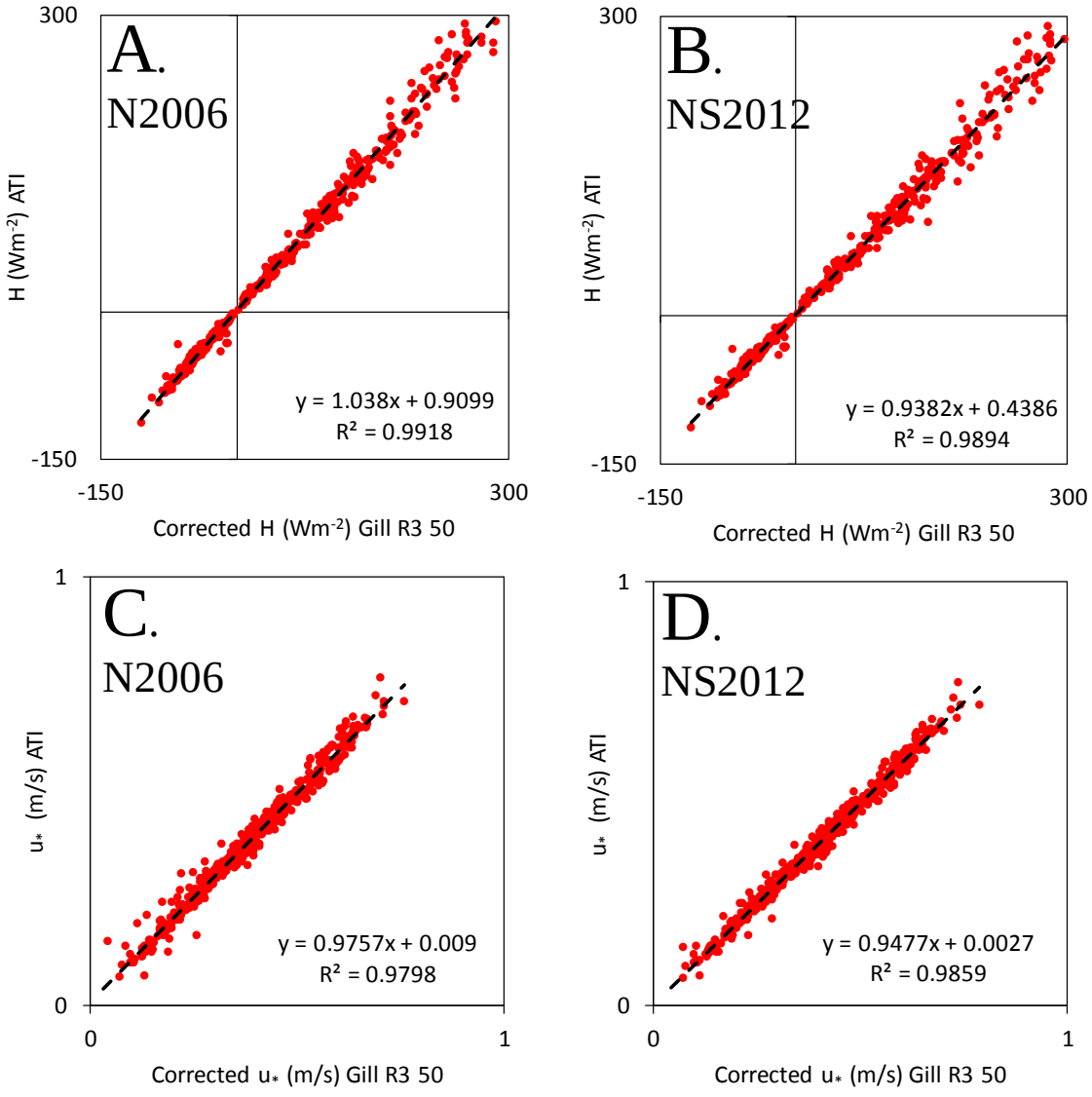

Figure 4-15. Comparison of ATI Vx and Gill R3 50 angle of attack corrected fluxes for A) sensible heat flux (H) with the N2006 correction, B) sensible heat flux with the NS2012 correction, C) friction velocity (u*) with the N2006 correction, and D) friction velocity with the NS2012 correction. Data are from June 17th to October 2nd, 2014. See text for details on the N2006 and NS2012 angle of attack corrections.

4.4 Further Analyses

The simple comparison setup of these three sonic anemometers run for a growing season and subsequent fallow/winter/spring period allowed for some unique additional phenomena to be evaluated with respect to the flow distortion. The first was to detect any impact of low temperatures on the magnitude of the underestimation of sensible heat flux and friction velocity. Electronics and physical structure are somewhat sensitive to wide ranges in temperatures and we could evaluate any impact on observed flux underestimations. The second was a comparison of fluxes for wind directions where flow was through the mounting structure of the ATI Vx anemometer. The Gill R3 sensors are omnidirectional and would be expected to show good agreement for north winds, while it is unclear how much the mounting structure would impact fluxes measured with the ATI Vx probe. Finally, the Gill R3 anemometers have an internal correction, developed from wind tunnel data, applied to generate "calibrated" u/v/w output. We turned this correction on and off and evaluated the resulted impact on sensible heat fluxes and friction velocity.

4.4.1 Flow distortion sensitivity to temperature

We examined the dataset for any dependence of the correction factor on temperature. Given the high correlation coefficients and small intercept values in Fig 4-11A and 4-13A for sensible heat flux and friction velocity, respectively, it is possible to compare these data in relation to ambient temperature. For acceptable fluxes (with no angle of attack corrections), we calculated a ratio of the half hourly H flux from the ATI Vx to that from the Gill R3 50 and Gill R3 100 and plotted values as a function of ambient air temperature for $|H| > 30$ W m^{-2} (so ratios would not be unreasonable due to a

division by a small number). The same procedure was carried out for u_* with minimum values greater than 0.1 m s^{-1}. We noted there was considerable scatter in the ratios (Fig. 4-16A and 4-16B) and therefore binned half hourly data in 10°C intervals of ambient temperature (-10 to 40 °C). However, no significant sensitivity of the H or u* ratio to temperature was observed suggesting flow distortion was not temperature sensitive.

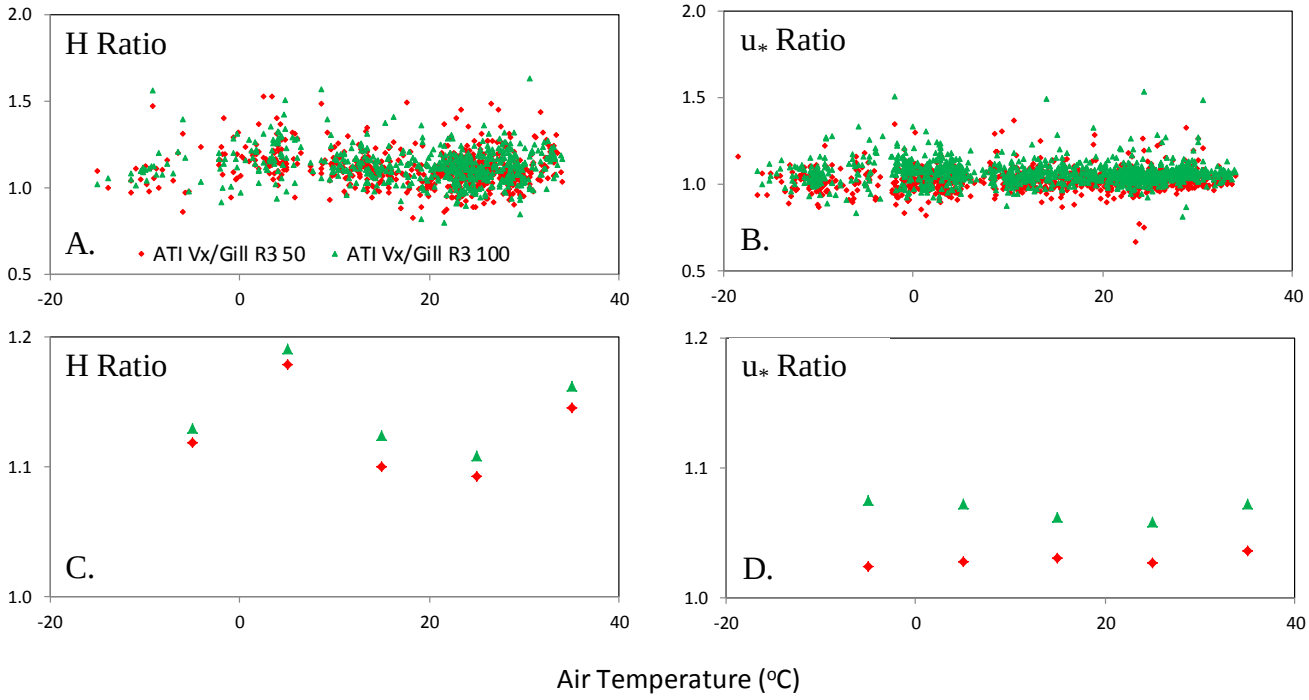

Figure 4-16 Ratios of fluxes of ATI Vx to R3 50 (or R3 100) as a function of air temperature for A) sensible heat flux (half hourly ratios), B) friction velocity (half hourly fluxes), C) binned sensible heat flux, and D) binned friction velocity (see text for details).

4.4.2 Flow distortion by ATI mounting structure

To examine flow distortion for winds flowing from behind the ATI Vx (i.e., through the mounting structure), the initial flux dataset was now screened using alternate wind direction criteria: only winds from 360° ± 20° were acceptable. No angle of attack corrections were applied to the fluxes. The two Gill R3 sensible heat fluxes continued to

agree well with each other for these wind directions (Fig. 4-17A; slope for H comparison is 0.99 and R^2 is 0.90). However, the H slope between the ATI Vx and the Gill R3 anemometers changed dramatically. For the Gill R3 50, the slope decreased from 1.11 (Fig. 4-11A) to 0.81 (Fig 4-17B). The correlation was still very strong ($R^2 = 0.87$). This is almost a 30% change in the relationship and the slope has changed from greater than one to less than one (i.e., Gill R3 H flux is now larger than the ATI Vx H flux). To explore this dramatic shift a little further, we changed the acceptable wind criteria to two other ranges ($220^o \pm 20^o$ and $320^o \pm 20^o$) and determined the slope for H fluxes between the ATI Vx and the Gill R3 50 (Fig. 4-18). We acknowledge for the two other ranges of wind direction, we may be seeing some impact of interference between sonic anemometers. But for winds from the northwest ($320^o \pm 20^o$), there is only a slight reduction in the slope between the sonic H fluxes (from 1.11 to 1.04). This result suggests fluxes measured for winds from directly behind the ATI Vx probe ($\pm 20^o$), should be removed in the flux screening process. However, the structure supporting the ATI Vx probe was minimal in this study (see Fig. 3-4) so the flow distortion was primarily from the mounting structure. In a configuration where the anemometer is supported by an eddy covariance tower, the impact on fluxes could be even greater and require a wider range of "non-acceptable" wind directions.

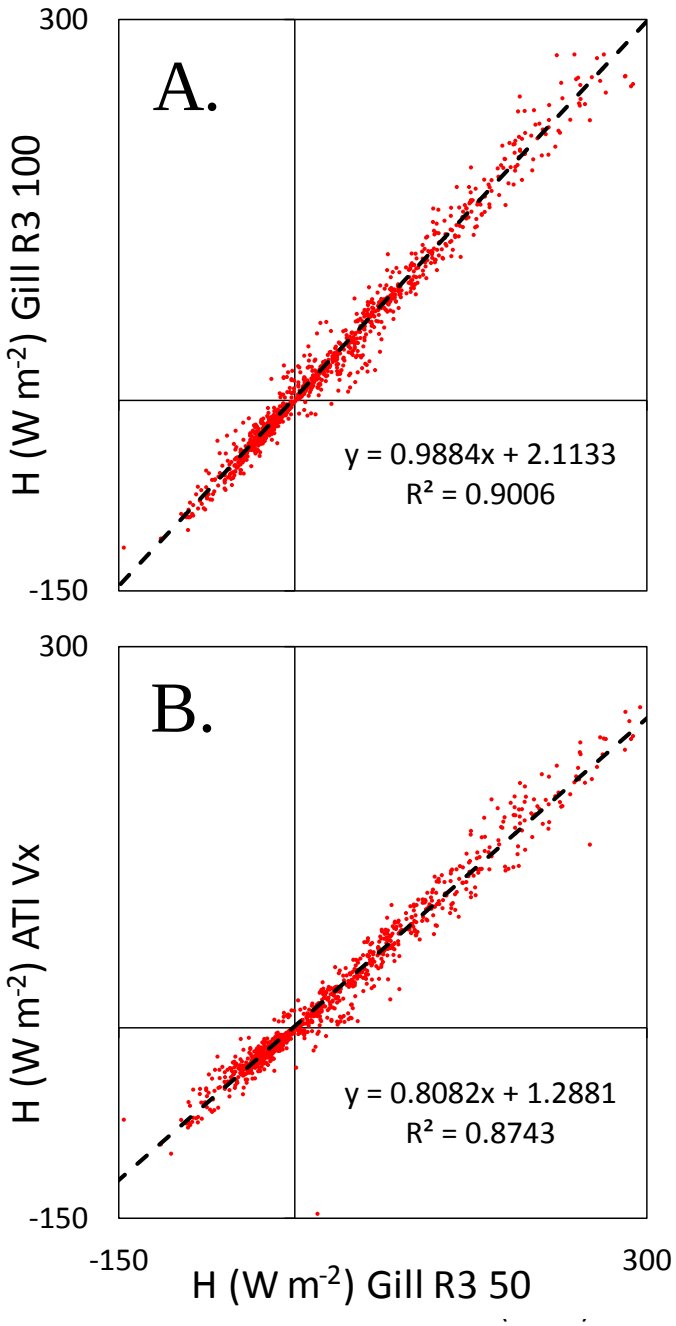

Figure 4-17. Comparison of sensible heat flux (H) during periods with northerly winds (winds that come directly from behind the ATI support structure) between A) the Gill R3 100 and Gill R3 50 and B) ATI Vx and Gill R3 50.

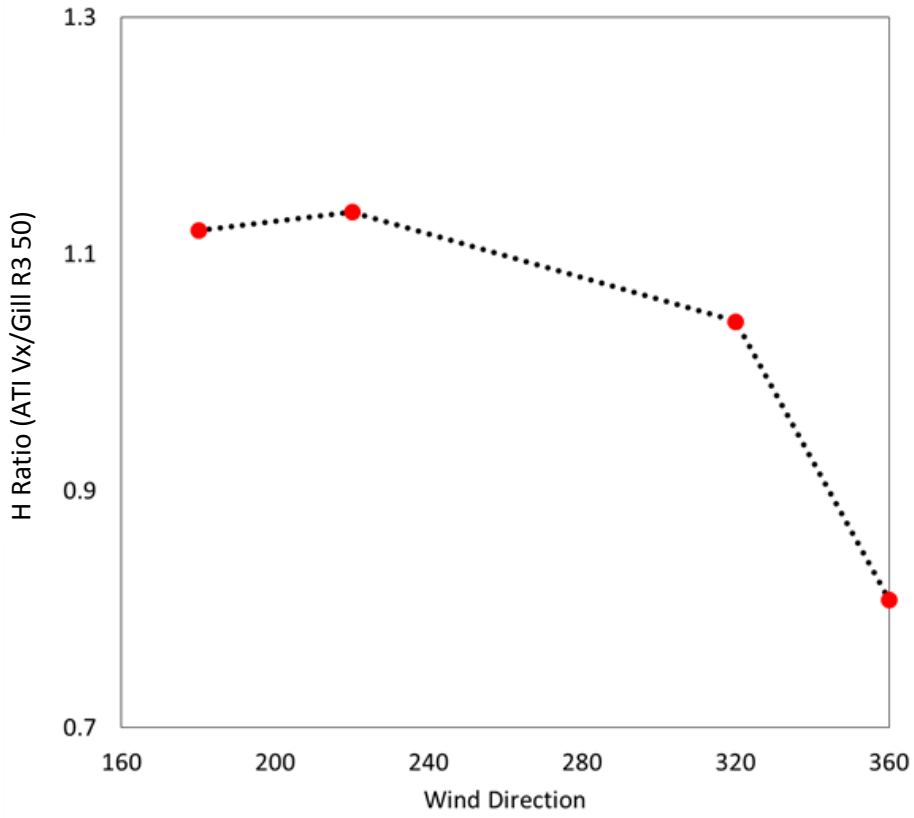

Figure 4-18. Ratio of sensible heat flux (H) for the ATI Vx and Gill R3 50 anemometers as a function of wind direction.

4.4.3 Gill internal corrections

For a period of 21 days in April 2015, the internal corrections in the Gill R3 100 were turned off (disabled) using Gill software. The output of this anemometer was therefore an uncalibrated but coordinate-rotated u, v, and w (and T_s). After the screening criteria were applied, 102 half hours of data were available for comparison. No angle of attack corrections were applied to the fluxes. In this configuration, the Gill R3 50 sensible heat fluxes which had compared quite well to the Gill R3 100 (slope of 0.99 and R^2 of 0.99; Fig. 4-11), now demonstrated a significant decrease in magnitude (slope of

0.89 and R^2 of 0.98; Fig. 4-19A). A similar decrease between the "calibrated" and "uncalibrated" friction velocity was measured (slope of 0.88 and R^2 of 0.97; Fig. 4-19B). These results demonstrate the significant impact internal corrections have on the magnitude of u, v, and w and subsequent fluxes for the Gill R3 sonic anemometers. As angle of attack corrections have been developed for the "calibrated" mode, they will not fully correct measured fluxes collected in the "uncalibrated" mode. We note the magnitude of these corrections for calibrated mode will vary to some degree among Gill R3 anemometers as each sensor is individually calibrated (i.e., measured horizontal flow for each anemometer is corrected to known laminar flow in a wind tunnel as the sonic is horizontally rotated; T. Stickland, *personal communication*).

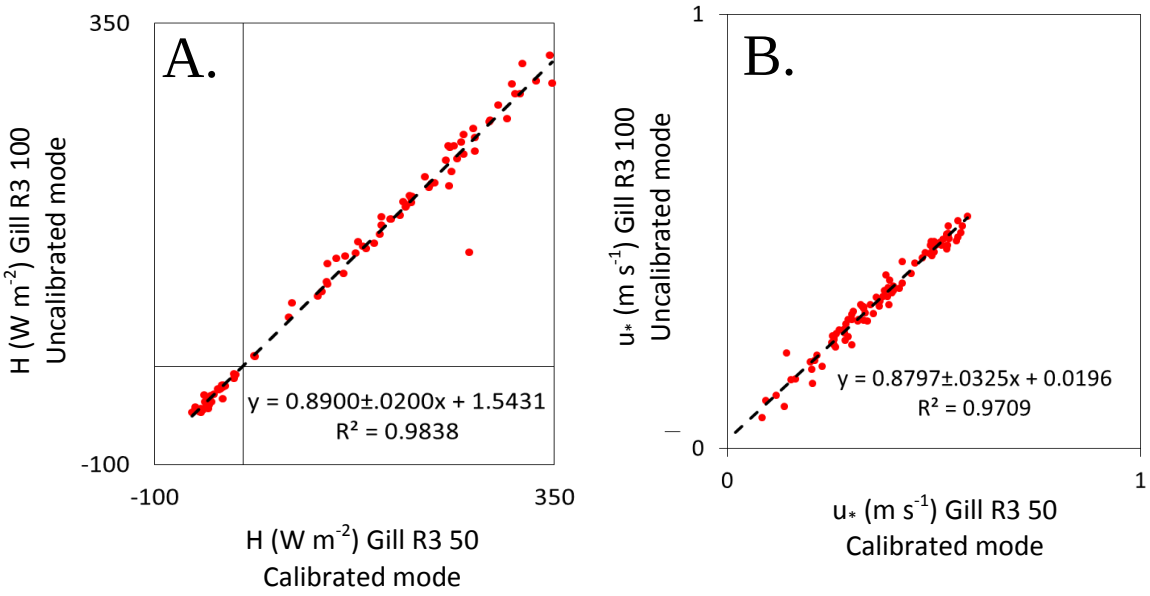

Figure 4-19. Comparison of A) sensible heat fluxes (H) calculated with a Gill R3 100 with internal corrections disabled (Uncalibrated mode) and Gill R3 50 with internal corrections enabled (Calibrated mode) and B) the same configuration for friction velocities (u_*). Data are from April 11th to May 1st, 2015.

Chapter 5 Conclusions

5.1 Non-orthogonal flow distortion impact on fluxes

5.1.1 Turbulent statistics and fluxes

This experimental design was focused on the impact of flow distortion for non-orthogonal sonic anemometers on fluxes and turbulent statistics. To our understanding, the omnidirectional models of Gill sonic anemometer (the Gill R3 100 and Gill R3 50) with the most current versions of firmware have not been compared to an orthogonal anemometer (ATI Vx) over a relatively smooth surface (an agricultural crop). For these data, collected during most of a soybean growing season and over the subsequent fall/winter, the standard deviation of vertical velocity was underestimated by ~5% while that for rotated horizontal velocity was overestimated by ~5%. There was ~12% underestimation of non-orthogonal sensible heat flux and ~ 5% for friction velocity compared to the orthogonal design. The results from this field experiment are consistent with previous studies examining the issue of flow distortion associated with non-orthogonal transducer design. These studies a) have been carried out in contrasting ecosystems for multiple models of non-orthogonal sonic anemometers and b) demonstrate how the physical characteristics of the measurement (canopy height, measurement height, surface roughness, etc.) impact fluxes due to flow distortion. These results also support the hypothesis that the ultrasonic anemometer design plays at least a partial role in a lack of energy balance closure at eddy covariance flux sites.

5.1.2 Angle of attack corrections

Two angle of attack corrections developed for the Gill omnidirectional ultrasonic anemometers were tested to determine how well they accounted for measured fluxes affected by non-orthogonal flow distortion. The first correction (N2006) was developed from Gill R2/R3 data collected from laminar wind tunnel flow using older versions of firmware. After applying this angle of attack correction, sensible heat fluxes continued to be underestimated by 4% (friction velocity was slightly overestimated by about 2%). The second correction (NS2012) was developed using Gill Windmaster (Pro) data collected in the field during turbulent flow. This procedure overcorrected the fluxes by 5% and 6% for the sensible heat flux and friction velocity, respectively. It was recently discovered and is being investigated and confirmed that firmware issues with vertical velocity in the Gill Windmaster (Pro) anemometer may have increased the magnitude of the correction. Therefore, the correction procedure will be significantly complicated as the user will need to know and have records of the model and firmware version to make current and correction to historical data.

5.1.3 Wind direction

We examined fluxes when the wind was blowing directly from behind the orthogonal anemometer through its mounting structure (i.e., 360° ± 20°). In contrast to southerly flow (180° ± 20°) when sensible heat flux from the orthogonal anemometer was about 11% higher than the omnidirectional non-orthogonal instrument, now fluxes were lower by ~20%. This ~31% discrepancy is attributed to the mounting structure. The "tower" in this experiment was a single pole so a more traditional eddy covariance tower could distort flow and reduce fluxes by even more. Not only does the sonic transducer

influence measurements of vertical wind speed and fluxes, but the instrument mounting boom associated with a sonic anemometer also has an impact, potentially greater than the effect introduced by the transducer arms.

5.1.3 Instrument internal corrections

The sonic anemometers used in this study have user-selectable settings. For the Gill R3 model, a calibrated, coordinate rotated output may be chosen. This is the most common output selected for typical eddy covariance measurements. We collected a portion of data with this calibration turned off in one of the two Gill R3 sonics (i.e., uncalibrated, coordinate rotated output) to examine the magnitude of the calibration. Sensible heat fluxes in the calibrated mode were ~12% higher compared to the uncalibrated mode. This result demonstrates internal corrections can have a significant impact on the magnitude of fluxes independent of flow distortion. Users must have knowledge of the implications of multiple internal settings on output and be aware of which internal settings are enabled.

5.2 Suggestions for further study

Based on the results from this study, there are some additional topics that can be explored in more detail:

A) *An analysis of the impact of non-orthogonal flow distortion on sonic temperature and subsequently sensible heat flux*. It is unclear to what extent flow distortion distorts sonic temperature and if this will affect sensible heat flux. The Gill R3 sonic anemometers use transit time from the three axes to calculate an average

sonic temperature. Each axis transit time has been affected by a) flow distortion and b) crosswind flow. Quantifying the magnitude of any bias in sonic temperature in non-orthogonal anemometers needs to be examined.

B) *An analysis of the interaction between flow distortion and wind direction*. We limited wind direction to the south for most of the analysis in this study. Furthermore, support structure was shown to significantly reduce fluxes. What is unclear is if the wind approaches the sonic anemometer from other wind directions, will the non-orthogonal design cause more or less flow distortion. Flux comparisons should be made from a range of different wind directions.

C) *Analysis of data during non-stationary turbulent flow*. During this study, periods that did not meet stationarity criteria (on the Foken 0-1-2 scale) were discarded. An examination of results from periods that did not meet stationarity criteria would provide additional insights into the nature of flow distortion impact. An analysis could be performed that examines the relationships between statistics of wind speed components, temperature, and fluxes during different periods with varying conditions.

Appendix

Program to record data on CR3000 Micrologger

```
PipeLineMode
Const SCAN_INTERVAl = 100
Const OUTPUT_INTERVAL = 30
Const SCAN_BUFFER_SIZE = 60*INT(1000/SCAN_INTERVAl)
'**************************
' ***** Variables ******
'**************************
Public OutStat As Boolean, LastFileName As String * 25
Public tp
Public ComStatus(3)
Public r3w(6)
Public r3e(6)
Public RT(9)
Public atis(4)
Dim n
Units n = samples
Dim r3w_str As String * 200
Dim ati_str As String * 500
Dim r3e_str As String * 200
Dim nmbr_bytes_rtrnd
Dim disable_flag As Boolean
Dim save_ts_on As Boolean
DataTable(Andyts,save_ts_on,-1)
        DataInterval (0,SCAN_INTERVAl, mSec, 220)
 CardOut(0,-1)
        Sample(6, RT(1),IEEE4)
        Sample(1,tp,IEEE4)
        Sample(6,r3w(1),IEEE4)
        Sample(6,r3e(1),IEEE4)
        Sample(4,atis(1),IEEE4)
EndTable
BeginProg
        n = 1
 SerialOpen (Com1,9600,3,0,300)
 ComStatus(1) = ComPortIsActive (Com1)
 SerialOpen (Com3,9600,3,0,300)
 ComStatus(2) = ComPortIsActive (Com3)
 SerialOpen (Com4,9600,10,0,300)
 ComStatus(3) = ComPortIsActive (Com4)
        Scan (SCAN_INTERVAl,mSEc,SCAN_BUFFER_SIZE,0)
          PanelTemp(tp,250)
                SerialInRecord (Com1,r3w_str,&h02,0,&h03,nmbr_bytes_rtrnd,01)
                SerialInRecord (Com3,r3e_str,&h02,0,&h03,nmbr_bytes_rtrnd,01)
                atis(1)=Mid(ati_str,1,7)
                atis(2)=Mid(ati_str,10,7)
                atis(3)=Mid(ati_str,19,7)
                atis(4)=Mid(ati_str,28,6)
                SplitStr (r3w(1),r3w_str,",",6,0)
                SplitStr (r3e(1),r3e_str,",",6,0)
                RealTime(RT())
          If (NOT(save_ts_on)) AND (IfTime(0,1,Min)) Then (save_ts_on = true)
                CallTable Andyts
        NextScan
EndProg
```

Chapter 6 Bibliography

Applied Technologies, Inc. Operators Manual For A Sonic Anemometer/Thermometerr. Revision J3. *Applied Technologies, Inc.*

Baldocchi, D. D. (2003). Assessing the eddy covariance technique for evaluating carbon dioxide exchange rates of ecosystems: Past, present and future. *Global Change Biology, 9*(4), 479-492.

Baldocchi, D., Falge, E., Gu, L., Olson, R., Hollinger, D., Running, S., et al. (2001). FLUXNET: A new tool to study the temporal and spatial variability of ecosystem-scale carbon dioxide, water vapor, and energy flux densities. *Bulletin of the American Meteorological Society, 82*(11), 2415-2434.

Burba, George. Eddy covariance method for scientific, industrial, agricultural and regulatory applications: A field book on measuring ecosystem gas exchange and areal emission rates. Li-Cor Biosciences, 2013.

Christen A, Gorsel Ev, Andretta M, Calanca P, Rotach MW, Vogt R (2000) Intercomparison of ultrasonic anemometers during the map Riviera project. Paper presented at ninth conference mountain meteorology, Snowmass Village, CO, August, 2000

Foken, T. (2008). The energy balance closure problem: An overview. *Ecological Applications, 18*(6), 1351-1367.

Frank, J. M., Massman, W. J., & Ewers, B. E. (2013). Underestimates of sensible heat flux due to vertical velocity measurement errors in non-orthogonal sonic anemometers. *Agricultural and Forest Meteorology, 171*, 72-81.

Gash, J., & Dolman, A. (2003). Sonic anemometer (co) sine response and flux measurement: I. the potential for (co) sine error to affect sonic anemometer-based flux measurements. *Agricultural and Forest Meteorology, 119*(3), 195-207.

Gill R3 and R3A User's Manual. Gill Instruments Ltd. (2004) *Gill Instruments Ltd.*

Horst, T., Semmer, S., Maclean, G., (2015) Correction of a Non-orthogonal Three-Component Sonic Anemometer for Flow Distortion by Transducer Shadowing. *Boundary-Layer Meteorology,* 155(3), 371-395

Kaimal, J. (1978). Sonic anemometer measurement of atmospheric turbulence. *Proceedings of the Dynamic Flow Conference 1978 on Dynamic Measurements in Unsteady Flows,* pp. 551-565.

Kaimal, J. (2013) Advances in Meteorology and the Evolution of Sonic Anemometry. http://www.apptech.com/history.html

Kaimal, J., & Businger, J. (1963). A continuous wave sonic anemometer-thermometer. *Journal of Applied Meteorology, 2*(1), 156-164.

Kaimal, J., & Gaynor, J. (1991). Another look at sonic thermometry. *Boundary-Layer Meteorology, 56*(4), 401-410.

Kaimal, J., Wyngaard, J., Izumi, Y., & Coté, O. (1972). Spectral characteristics of surface-layer turbulence. *Quarterly Journal of the Royal Meteorological Society, 98*(417), 563-589.

Kochendorfer, J., Meyers, T. P., Frank, J. M., Massman, W. J., & Heuer, M. W. (2013). Reply to the comment by mauder on "How well can we measure the vertical wind speed? Implications for fluxes of energy and mass". *Boundary-Layer Meteorology, 147*(2), 337-345.

Kochendorfer, J., Meyers, T. P., Frank, J., Massman, W. J., & Heuer, M. W. (2012). How well can we measure the vertical wind speed? Implications for fluxes of energy and mass. *Boundary-Layer Meteorology, 145*(2), 383-398.

Liu, H., Peters, G., & Foken, T. (2001). New equations for sonic temperature variance and buoyancy heat flux with an omnidirectional sonic anemometer. *Boundary-Layer Meteorology, 100*(3), 459-468.

Metzger, M., McKeon, B. J., & Holmes, H. (2007). The near-neutral atmospheric surface layer: turbulence and non-stationarity. Philosophical Transactions of the Royal Society A: Mathematical, Physical and Engineering Sciences, 365(1852), 859-876.

Moncrieff, J. B., Massheder, J. M., De Bruin, H., Elbers, J., Friborg, T., Heusinkveld, B., ... & Verhoef, A. (1997). A system to measure surface fluxes of momentum, sensible heat, water vapour and carbon dioxide. Journal of Hydrology, 188, 589-611.

Nakai, T., Iwata, H., Harazono, Y., & Ueyama, M. (2014). An inter-comparison between Gill R3 50nd campbell sonic anemometers. *Agricultural and Forest Meteorology, 195*, 123-131.

Nakai, Taro, and Kou Shimoyama. "Ultrasonic anemometer angle of attack errors under turbulent conditions." *Agricultural and forest meteorology* 162 (2012): 14-26.

Nakai, T., Van Der Molen, M., Gash, J., & Kodama, Y. (2006). Correction of sonic anemometer angle of attack errors. *Agricultural and Forest Meteorology, 136*(1), 19-30.

Rosenberg, N. J., Blad, B. L., & Verma, S. B. (1974). *Microclimate: The biological environment* Wiley New York.

Schotanus, P., Nieuwstadt, F., & De Bruin, H. (1983). Temperature measurement with a sonic anemometer and its application to heat and moisture fluxes. *Boundary-Layer Meteorology, 26*(1), 81-93.

Schotland, R. (1955). The measurement of wind velocity by sonic means. *Journal of Meteorology, 12*(4), 386-390.

Van der Molen, M., Gash, J., & Elbers, J. (2004). Sonic anemometer (co) sine response and flux measurement: II. the effect of introducing an angle of attack dependent calibration. *Agricultural and Forest Meteorology, 122*(1), 95-109.

Van Dijk, A., Moene, A., & De Bruin, H. (2004). The principles of surface flux physics: Theory, practice and description of the ECPACK library. *Meteorology and Air Quality Group, Wageningen University, Wageningen, the Netherlands*, , 99.

Weiss, A., & Allen, L. H. (1976). The flux-angle distribution of momentum as determined from propeller anemometer measurements. Quarterly Journal of the Royal Meteorological Society, 102(434), 775-779.

Wilson, K., Goldstein, A., Falge, E., Aubinet, M., Baldocchi, D., Berbigier, P., et al. (2002). Energy balance closure at FLUXNET sites. *Agricultural and Forest Meteorology*, *113*(1), 223-243.

Wyngaard, J. (1981). Cup, propeller, vane, and sonic anemometers in turbulence research. *Annual Review of Fluid Mechanics*, *13*(1), 399-423.

Wyngaard, J. C., & Zhang, S. (1985). Transducer-shadow effects on turbulence spectra measured by sonic anemometers. *Journal of Atmospheric and Oceanic Technology*, *2*(4), 548-558.

Yuling, F. (2005). Energy balance closure at ChinaFLUX sites.